Enhanced upper ocean stratification with climate change in the CMIP3 models

Antonietta Capotondi,[1,2] Michael A. Alexander,[2] Nicholas A. Bond,[3] Enrique N. Curchitser,[4] and James D. Scott[1,2]

Received 25 June 2011; revised 2 March 2012; accepted 6 March 2012; published 25 April 2012.

[1] Changes in upper ocean stratification during the second half of the 21st century, relative to the second half of the 20th century, are examined in ten of the CMIP3 climate models according to the SRES-A2 scenario. The upper ocean stratification, defined here as the density difference between 200 m and the surface, is larger everywhere during the second half of the 21st century, indicative of an increasing degree of decoupling between the surface and the deeper oceans, with important consequences for many biogeochemical processes. The areas characterized by the largest stratification changes include the Arctic, the tropics, the North Atlantic, and the northeast Pacific. The increase in stratification is primarily due to the increase in surface temperature, whose influence upon density is largest in the tropical regions, and decreases with increasing latitude. The influence of salinity upon the stratification changes, while not as spatially extensive as that of temperature, is very large in the Arctic, North Atlantic and Northeast Pacific. Salinity also significantly contributes to the density decrease near the surface in the western tropical Pacific, but counteracts the negative influence of temperature upon density in the tropical Atlantic.

Citation: Capotondi, A., M. A. Alexander, N. A. Bond, E. N. Curchitser, and J. D. Scott (2012), Enhanced upper ocean stratification with climate change in the CMIP3 models, *J. Geophys. Res.*, *117*, C04031, doi:10.1029/2011JC007409.

1. Introduction

[2] The upper ocean stratification plays a key role in many ocean biogeochemical processes. In particular, mixed layer depth (MLD) regulates the interplay between light availability for photosynthesis and nutrient supply from the deep to upper oceans. Light availability and nutrient levels, whose relative importance is region dependent, are major factors in biological productivity. The density gradient at the base of the mixed layer affects entrainment processes, which play a crucial role in mixed layer deepening and in supplying nutrients to the euphotic zone. The upper ocean stratification, defined here as the density difference between the mixed layer and the deep ocean, can also influence ocean ventilation, the process by which surface quantities are injected, or "subducted," into the ocean interior, with important consequences for the oceanic uptake of carbon and oxygen.

[3] Some studies have examined the influence of global warming upon MLD in the North Pacific [*Merryfield and Kwon*, 2007; *Luo and Rothstein*, 2009; *Jang et al.*, 2011], and in the Southern Ocean [*Sen Gupta et al.*, 2009]. Overall, MLDs are projected to shoal in these two regions, with the largest changes found in the areas of climatological deepest mixed layers, such as the Subtropical Gyre in the North Pacific. In the Southern Ocean, the MLD shoals in a broad band extending from the central Indian Ocean southwestward toward the Drake Passage and continuing to the western South Atlantic. However, in many areas, the MLD projected changes are relatively small, as illustrated in Figure 1 for four of the climate models participating in the Climate Model Intercomparison Project version 3 (CMIP3) at a location in the northeast Pacific (∼50°N, 145°W). Figure 1 compares winter (JFM) vertical density profiles averaged over the period 1950–1999 (20th century simulation, solid line) with the profiles averaged over the period 2050–2099 for the 21st century simulations according to the Special Report on Emissions Scenarios (SRES) A2 scenario (dot-dash line). The MLD varies among the models, as seen by visual inspection (Figure 1), ranging from 60 to 70 m in the GFDL-CM2.1 and CGCM3.1(T47) models to ∼100 m in CCSM3 and UKMO-HadCM3. While the depth of the mixed layer does not seem to change appreciably in Figure 1, the density gradient at the base of the mixed layer is much larger during the second half of the 21st century, indicative of an increasing tendency for the upper ocean to decouple from the deep ocean. In this study we will focus upon this vertical density gradient, and will examine how it is projected to change over the World Ocean as a consequence of global warming.

[1]CIRES, University of Colorado Boulder, Boulder, Colorado, USA.
[2]Physical Science Division, Earth System Research Laboratories, NOAA, Boulder, Colorado, USA.
[3]Joint Institute for the Study of the Atmosphere and Ocean, University of Washington, Seattle, Washington, USA.
[4]Institute of Marine and Coastal Sciences, Rutgers, State University of New Jersey, New Brunswick, New Jersey, USA.

0148-0227/12/2011JC007409

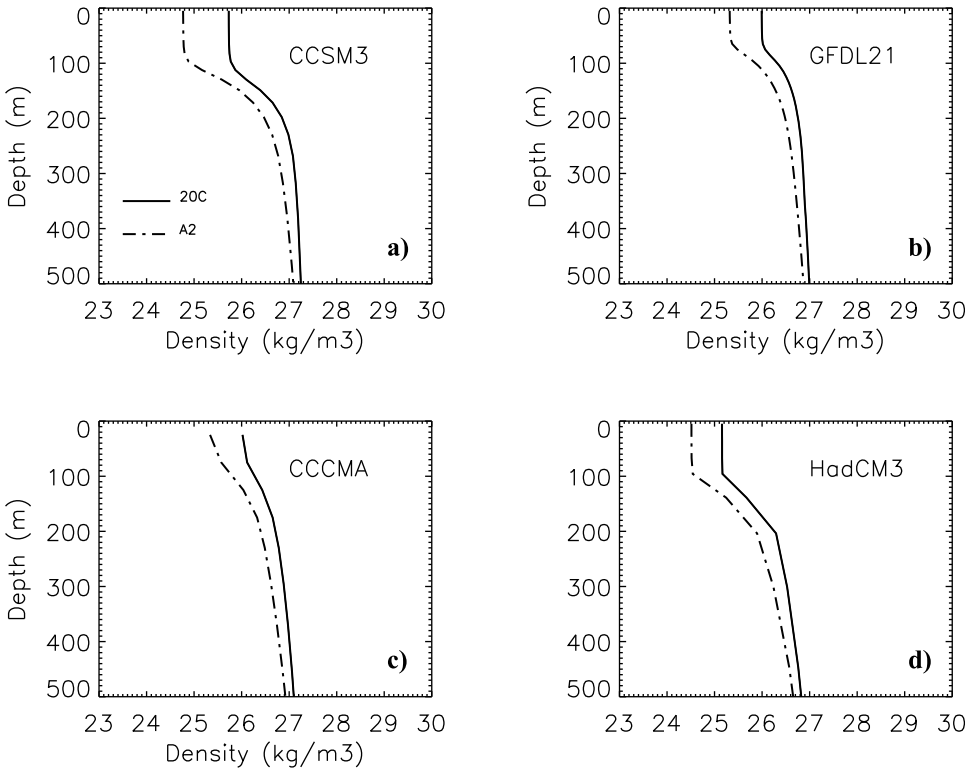

Figure 1. Winter (JFM) vertical density profiles at the location of Ocean Weather Station Papa (50°N, 145°W) for four of the CMIP3 climate models: (a) CCSM3, (b) GFDL-CM2.1, (c) CGCM3.1(T47), and (d) UKMO-HadCM3. The profiles are averaged over the period 1950–1999 (solid lines), and 2050–2099, according to the SRES-A2 scenario (dot-dash lines). Potential density values are relative to 1000 kg m^{-3}.

[4] In a pioneering study with an earlier version of the Geophysical Fluid Dynamics Laboratory (GFDL) climate model, coupled to a carbon cycle model, *Sarmiento et al.* [1998] found that the projected decrease of oceanic uptake of CO_2 in the 21st century had a strong high-latitudes signature, and was particularly large in the Southern Hemisphere. The primary reason for those high-latitude changes was not the decreased rate of deep-water formation, but the increased stratification of the upper water column. In fact, the density gradient at the base of the first model layer showed a large positive trend in a global average sense, and was accompanied by a decrease of the global mean oceanic oxygen, which was suggested by *Sarmiento et al.* [1998] as a possible tracer of the changes in the carbon balance.

[5] Oceanic oxygen observations show concentration declines in many areas of the World Ocean, with the North Pacific and tropical oceans being the best resolved regions due to the availability of long-term moorings and repeated hydrographic sections [*Sarmiento et al.*, 1998]. In particular, time series from mid-depth waters at station Papa (50°N, 145°W) show long-term declines of 7 μmol/kg/decade as well as shoaling of the level of hypoxia (taken as the 60 μmol/kg surface) over the period 1956–2006 [*Whitney et al.*, 2007]. Similar changes are observed in the California Current System during 1984–2006 [*Bograd et al.*, 2008] and in the Oyashio Current region off Japan [*Ono et al.*, 2001; *Watanabe et al.*, 2003]. The mid-depth changes in the Oyashio Current region appear to be correlated with those observed at station Papa, with a lead of about 7 years, an indication of the possible role of advective processes. In the Tropics, *Stramma et al.* [2008] have constructed time series of oxygen over selected regions in the tropical Atlantic, Pacific, and Indian Oceans using both historical and recent observations. Oxygen declines were found in the 300–700 m depth range, together with a vertical expansion of the zone of hypoxia. A comprehensive list of the observational studies documenting oxygen changes is provided by *Keeling et al.* [2010]. All the observed changes appeared to be related to variations in physical quantities, such as ocean stratification, ventilation, and circulation, rather than changes in oxygen utilization [*Dore et al.*, 2003, 2009]. Given the fundamental role played by oxygen in the biogeochemical cycle, it is very important to understand the influence of climate change upon ocean stratification and circulation.

[6] In this study we use a subset of the climate simulations performed in the context of the Coupled Model Intercomparison Project Phase 3 (CMIP3) [*Meehl et al.*, 2007], and used for the Intergovernmental Panel on Climate Change Fourth Assessment Report (IPCC-AR4) to examine the changes in upper ocean stratification over the second half of the 21st century relative to the second half of the 20th century.

Table 1. List of the CMIP3 Models Used in This Study[a]

Model	Oceanic Model	Oceanic Resolution	Atmospheric Resolution	Reference
CGCM3.1 (T47)	MOM1.1	1.85° × 1.85°, L29	T47 L31	*Kim et al.* [2002]
CSIRO-Mk3.5	MOM2.2	0.84° × 1.875°, L31	T63 L18	*Gordon et al.* [2002]
GFDL-CM2.0	OM3P4	1°(1/3°) × 1°, L50	2.5° × 2°, L24	*Delworth et al.* [2006]
GFDL-CM2.1	OM3.1P4	1°(1/3°) × 1°, L50	2.5° × 2°, L24	
INGV-SXG	OPA8.2	2° × 2°(1°), L31	T106 L19	*Valcke et al.* [2000]
MIROC3.2 (medres)	COCO3.3	1.4°(0.5°) × 1.4°, L43	T42 L20	K-1 model developers 2004
ECHAM5/MPI-OM	MPI OM	1.5° × 1.5° L40	T63 L31	*Jungclaus et al.* [2006]
MRI-CGCM2.3.2	Bryan-Cox	2°(0.5°) × 2.5°, L23	T42 L30	*Yukimoto et al.* [2001]
CCSM3	POP	1.1°(0.27°) × 1.1°, L40	T85 L26	*Collins et al.* [2006]
UKMO-HadCM3	Bryan-Cox	1.25° × 1.25°, L20	2.75° × 3.75°, L19	*Gordon et al.* [2000]

[a]The standard CMIP3 IDs are used for the models. Information about ocean model components, oceanic and atmospheric resolutions, and relevant references documenting the models, are also included.

[7] Previous studies [*Liu et al.*, 2005; *Xie et al.*, 2010] have examined different aspects of sea surface temperature (SST) change due to global warming in different subsets of the CMIP3 models. In particular, *Xie et al.* [2010] have used a large ensemble of simulations performed with the Geophysical Fluid Dynamics Laboratory climate model (GFDL-CM2.1) and with the National Center for Atmospheric Research (NCAR) Community Climate System Model Version 3 (CCSM3) to identify patterns of SST changes, and relate them to changes in surface heat fluxes, wind stress and ocean dynamics.

[8] Global warming is also associated with changes in the hydrological cycle [*Allen and Ingram*, 2002; *Held and Soden*, 2006; *Richter and Xie*, 2010; *Stephens and Ellis*, 2008], with increased precipitation over the Tropics and high-latitudes, and decreased precipitation in the subtropical regions, so that sea surface salinity (SSS) changes can also be expected. Some observational studies [*Cravatte et al.*, 2009; *Durack and Wijffels*, 2010] have found large decreasing trends in the tropical Pacific and high-latitude regions over the second half of the 20th century and beginning of the 21st century, in qualitative agreement with the model projected changes in the hydrological cycle. Twenty-first century projections of the salinity fields from the CMIP3 models have been examined by *Terray et al.* [2012] in the Tropics. However, model projections over the Global Ocean have not been fully considered, and the relative influence of SST and SSS upon surface density and upper ocean stratification has also not been examined. Due to the nonlinearity of the equation of state, the influence of salinity upon density is dependent on temperature, and becomes increasingly larger at high-latitudes, where temperatures are colder. These high-latitude areas are also the regions where precipitation is projected to increase, and where a large reduction in SSS can be expected, possibly resulting in surface density decrease.

[9] The major goal of this study is to examine patterns of stratification change, identify areas where changes are particularly large, and clarify the relative role of SST and SSS in producing those patterns. The paper is organized as follows: In section 2 we describe the models and the analysis procedure. In section 3 we consider the changes in SST occurring over the second half of the 21st century versus the second half of the 20th century. Changes in SSS and their relationship to the surface freshwater fluxes are described in section 4, while changes in surface density and stratification are described in section 5. Conclusions are drawn in section 6.

2. Models and Methodology

[10] We examine simulations of the 20th century (20C3M) as well as simulations of the 21st century according to the Special Report on Emission Scenarios (SRES) A2 scenario, the high-forcing scenario characterized by CO_2 concentrations reaching a value of 820 PPM by year 2100 [*Nakićenović et al.*, 2000; *Meehl et al.*, 2007]. Most of the studies that have examined CMIP3 simulations have focused on the SRES-A1B scenario, which is characterized by intermediate greenhouse gas forcing [*Nakićenović et al.*, 2000]. The different scenarios start diverging appreciably around year 2020, so that it is uncertain which scenario can best represent the future CO_2 increase for the rest of the 21st century. The SRES-A2 scenario is used here as it can provide the best signal-to-noise ratio. The results obtained in this study can be qualitatively compared with similar analyses using the SRES-A1B simulations described in the literature, thus providing a broader perspective on the influence of climate change upon different upper ocean quantities.

[11] We use ten models, whose basic characteristics are listed in Table 1. The first criterion for the model's selection was the availability of both oceanic and atmospheric data needed for this study. Preliminary analyses of upper ocean density structure and MLD in the North Pacific and North Atlantic led us to the elimination of other models, due to their unrealistic MLDs in the North Pacific, also noted by *Jang et al.* [2011], or unrealistically extensive ice cover in the northwest Atlantic. Based on recent studies on the choice and use of multimodel ensembles [*Pierce et al.*, 2009; *Knutti et al.*, 2010; *Santer et al.*, 2009] we expect our ensemble to include enough members to produce meaningful and representative results. For example, *Pierce et al.* [2009] showed that for future average temperature over the western United States the ensemble skill approached the same asymptote once any 6 GCMs were included. Further, using a metric of precipitation trend, 11 randomly selected GCMs produced results almost identical to those using the 11 "best" GCMs [*Knutti et al.*, 2010], and detection and attribution of changes in atmospheric water vapor were insensitive to whether the "best" or "worst" 10 GCMs were used [*Santer et al.*, 2009].

[12] The model output has been downloaded from the Program for Climate Model Diagnosis and Intercomparison (PCMDI) archive. Since there is no consistency in the number of ensemble members among models and scenarios, only one ensemble member per model has been considered. For those models with more than one ensemble member, the first member (referred to as "run 1") has been chosen. The models used for the study differ in their horizontal and vertical resolutions, as shown in Table 1, and in their sub-grid scale parameterizations (see references, for each model, in Table 1). Among the ten models used, only CGCM3.1(T47) and MRI-CGCM2.3.2 use flux adjustments, heat and freshwater for CGCM3.1(T47), and heat, freshwater and momentum for MRI-CGCM2.3.2. All other models are not flux adjusted [*Randall et al.*, 2007].

[13] *Reichler and Kim* [2008], among others, have shown that the average of the multimodel ensemble is more similar to observations than any individual model, likely due to the compensation of individual model errors. For this reason, we will focus here upon ensemble average quantities, although it is not known whether the multimodel mean can provide the best future projection. In addition, examples of results from individual models will also be shown to illustrate the range of differences among models, and elucidate some of the processes involved. We have examined monthly values of upper ocean potential temperature, salinity, potential density, as well as surface wind stress, evaporation and precipitation. Evaporation has been obtained by dividing the surface latent heat flux by the latent heat of vaporization of water. Not all the models have density available in the PCMDI archive. Since we are interested in examining the relative contribution of potential temperature and salinity to the density and stratification changes, density has been computed from potential temperature and salinity using the nonlinear equation of state (EOS-80).

[14] To examine the changes in upper ocean stratification we consider the difference between density at 200 m and surface density. The use of 200 m as our reference depth seemed appropriate to characterize the upper ocean vertical density gradient. In most regions this depth is below the annually averaged MLD (see Figure 1 as an example), so that the vertical density difference provides an estimate of the density gradient at the base of the mixed layer. In other regions, like the subtropical gyres, the Southern Ocean and in the areas of the North Atlantic where deep convection occurs, the mixed layer can reach several hundreds meters, so our reference depth may lie within the mixed layer, and the criterion used cannot be interpreted as a measure of the changes in the density jump at the base of the mixed layer. However, the use of 200 m as a reference depth provides a good estimate of the upper ocean density gradients even in weakly stratified regions. The use of a deeper level (400 m) leads to very similar patterns of stratification changes (not shown).

[15] The results presented in this paper are primarily in the form of difference fields between the average conditions over the second half of the 21st century (2050–2099, Period2), and the second half of the 20th century (1950–1999, Period1). Trends over the 20th century and beginning of the 21st century are also computed for comparison with corresponding observational estimates. Since we are considering only one ensemble member per model, we have chosen 50 years, a relatively long averaging period, to define the changes in model climatology.

[16] Natural variability of the climate system occurs on decadal/multidecadal timescales. The "Inter-decadal Pacific Oscillation" (IPO) [*Power et al.*, 1999] or "Pacific Decadal Oscillation" (PDO) [*Mantua et al.*, 1997], as well as the Atlantic Multidecadal Oscillation (AMO) [*Enfield et al.*, 2001] are examples of modes of climate variability associated with multidecadal variations that could affect a 50-year mean. Based upon a 40-member ensemble of CCSM3 simulations for the period 2000–2060 according to the SRES-A1B scenario, *Deser et al.* [2010b] have shown that much of the uncertainty associated with climate change projections is due to internal climate variability. Thus, 50 years may not be a sufficiently long period to define mean conditions over the 20th and 21st centuries. In other words, not all of this variability is removed by averaging over 50 years for the purpose of defining mean conditions for the second halves of the 20th and 21st centuries.

[17] The model output at PCMDI only includes few ensemble members for each model, so that it is difficult to accurately quantify the influence of natural variability on the 50-year means for each model. To gain some insight on the influence of internal variability upon estimates of mean conditions and forced climate response, we use a 500 year Pre-Industrial control integration (PIcntrl) of CCSM3. CCSM3 is one of a few models, among those used in this study, with a long PIcntrl simulation available at PCMDI, and the study of *Deser et al.* [2010b] has provided a broad overview of the uncertainties in climate projections associated with internal variability in that model. Figure 2 shows the standard deviation of 50-year mean temperature (Figures 2a and 2c) and salinity (Figures 2b and 2d) fields, both at the surface (Figures 2a and 2b) and 200 m (Figures 2c and 2d), based upon ten non-overlapping 50-year segments of the PIcntrl simulation of CCSM3. Differences in mean conditions from segment to segment are entirely due to internal variability.

[18] Over most of the ocean standard deviations are smaller than 0.2°C for temperature, and 0.1 psu for salinity. For temperature, the regions where the spread is larger include the Kuroshio Extension, the Southern Ocean, from 150°W to 60°W, and the North Atlantic. At 200 m (Figure 2c), standard deviations of ~0.3–0.5°C are also seen in the North Pacific along bands extending southwestward from the northeastern basin. We will see in section 3 that the temperature changes (Period2-Period1) in the Kuroshio Extension are larger than the spread of the mean in the same area (Figure 7a). However, in the North Atlantic, variations of the mean can be as large as 1°C, both at the surface and at 200 m (Figures 2a and 2c), and represent a significant fraction of the temperature difference between Period2 and Period1 in CCSM3 (Figure 7a). In the Southern Ocean, the standard deviation of the 50-year mean, although smaller than in the North Atlantic, is also comparable to the period difference in Figure 7a.

2.1. Statistical Significance

[19] The use of multimodel ensembles for climate projections is relatively new, and has prompted several studies that discuss various approaches for determining the robustness

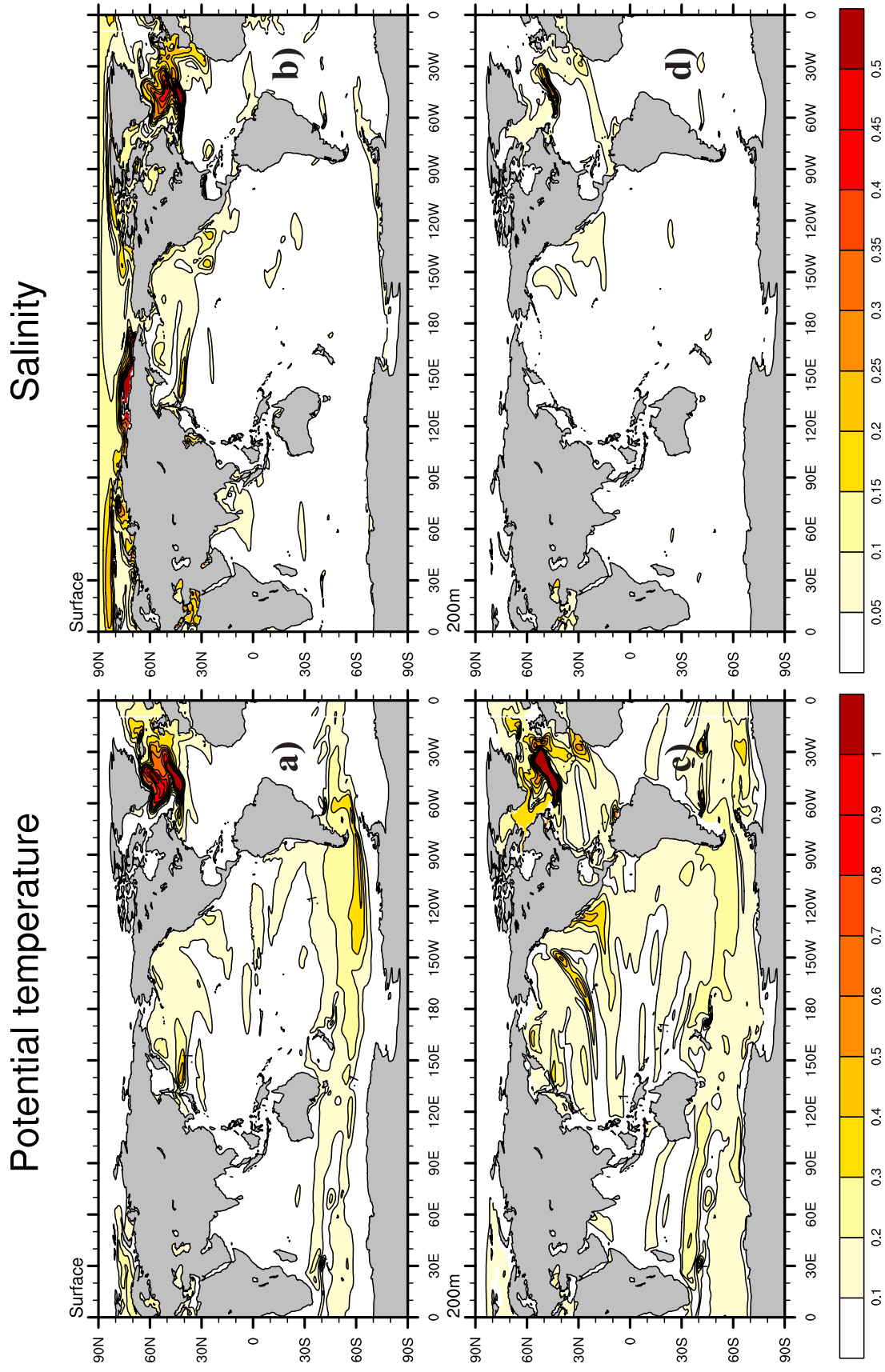

Figure 2. Standard deviation of 50-year means, computed from 10 non-overlapping segments of 500 year PIcntrl integration of CCSM3, for (a and c) potential temperature (°C) and (b and d) salinity (psu), at the surface (Figures 2a and 2b), and 200 m (Figures 2c and 2d).

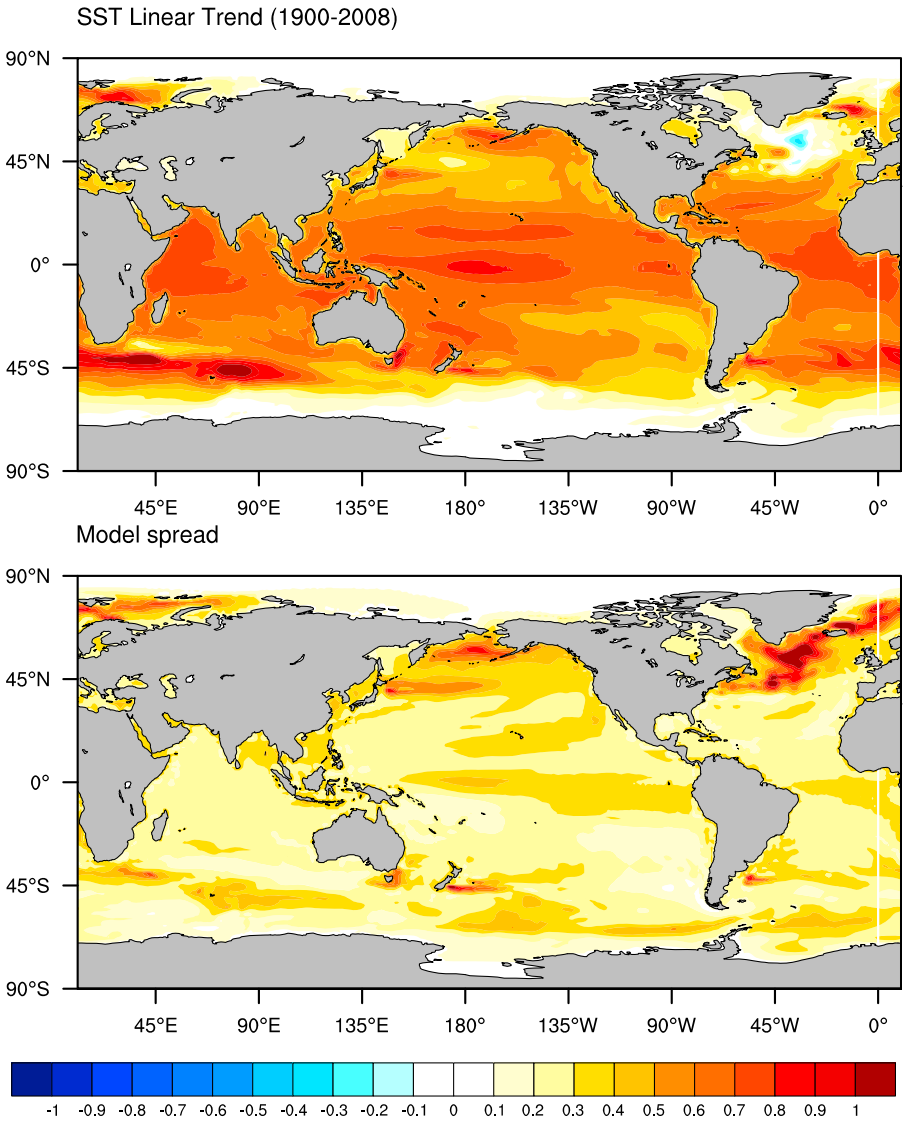

Figure 3. (top) Multimodel ensemble average of SST trend (°C per century) over the period 1900–2008. The 20th century simulations (20C3M) were used for 1900–2000, while the SRES-A2 scenario was used for 2000–2008. (bottom) Multimodel standard deviation of the trend.

and reliability of multimodel means [e.g., *Tebaldi and Knutti*, 2007; *Knutti et al.*, 2010; *Tebaldi et al.*, 2011]. Due to inter-model dependency, common biases, and limited representativeness of the sample of models with regard to fundamental uncertainties, the application of common statistical techniques based on model spread to determine statistical significance of multimodel means is questionable [*Tebaldi and Knutti*, 2007]. The approach adopted for some of the results presented in the IPCC-AR4 Summary for Policymakers [see, e.g., *Alley et al.*, 2007, Figure SPM.7] is to indicate areas where a certain percentage of models agree on the sign of the change. In this example changes were considered robust (as highlighted by stippling) where more than 90% of the models agreed on the sign of the change, while areas where less than 66% of the models agreed were left white. However, as pointed out by *Tebaldi et al.* [2011], models may disagree in areas where the signal-to-noise ratio is small, information that is important to retain. Instead, *Tebaldi et al.* [2011] suggest to first assess the statistical significance of each model in the ensemble. For locations where fewer than 50% of the model results have statistical significance, the simulated changes are essentially indistinguishable from "noise." For the remaining locations, the agreement in the sign of the changes among the models is considered. Stippling is used for the grid points where at least 80% of the models agree in sign, and white is used for the areas where less than 80% of the model agrees. The latter are areas where the signal is above the internal variability "noise" in each model, but there is large uncertainty across models. In this study, we have adopted the above procedure, as outlined by *Tebaldi et al.* [2011], to provide a measure of significance for the ensemble average period differences of potential temperature and salinity. The 95% statistical significance for each model is estimated relative to the standard deviation of the fields during Period1 and Period2, using a t-test approach [*Wilks*, 1995].

2.2. Model Drift

[20] Climate models are integrated forward in time from a set of initial conditions, and will "drift" from the initial state until a quasi-equilibrium state is reached. The CMIP3 archive includes pre-industrial control integrations that were carried out for several hundred years and provided initial conditions for the 20th century integrations, at the end of which the scenario simulations started. However, the adjustment of the deep ventilated ocean can take thousands of years to equilibrate, so that some model drift can be expected to be present and may affect our results. Some studies [*Cai and Gordon*, 1999; *Covey et al.*, 2006; *Sen Gupta et al.*, 2009] have addressed the issue of climate drift in climate models. In particular, *Sen Gupta et al.* [2009] have examined the magnitude of the drift in the CMIP3 archive, with focus upon the Southern Ocean. The drift was computed from a 100-year segment of the control integration overlapping with the 20th century simulations. For most models significant drifts were found below ~500 m, except for the INGV-SXG model which had large drift at all depths. It was also indicated that there is no systematic bias in the sign of the drift, since the drift was effectively removed by averaging across the models. The ensemble average drift was maximum around 1000 m. Thus, we expect that the results presented in this study, consisting of ensemble averages of fields in the upper ocean should be little affected by model drift.

3. Changes in the Temperature Field

[21] Validation of modeled SST trends is hampered by limitations in the observational record, including the availability of time series long enough to enable the detection of a small trend within a relatively large-amplitude natural variability. *Deser et al.* [2010a] have examined both reconstructed and un-interpolated data sets, and verified their consistency with related fields (surface air temperature, sea level pressure, precipitation and cloudiness) to assess the sign and magnitude of 20th century (1900–2008) SST trends. Apart from the eastern equatorial Pacific, which is not well-constrained by observations, all data sets examined by *Deser et al.* [2010a] show warming everywhere, except in the northwestern Atlantic [see *Deser et al.*, 2010a, Figure 1]. The magnitude of the warming varies among the different observational data sets, and is overall larger in the un-interpolated ones. All data sets show warming in the Southern Ocean within ~30°–50°S, especially in the Indian and Atlantic sectors, although the regional details differ among the various products. The areas of enhanced Southern Ocean warming are approximately located along the Subtropical Front (STF) [*Clifford*, 1983; *Hofmann*, 1985], separating the cold and fresh waters of the Southern Ocean from the saltier and warmer subtropical waters.

[22] The 1900–2008 SST trend for the ten models ensemble is shown in Figure 3 (top). The SRES-A2 scenario is used for the period 2000–2008. Consistent with the *Deser et al.* [2010a] results, a warming trend is found everywhere except in the North Atlantic, just South of Greenland, where the model ensemble average shows a weak cooling. The model ensemble average shows enhanced warming in the Tropics, in the North Pacific and in the Southern Ocean. While the North Pacific, Southern Ocean and tropical Atlantic warming are consistent with some of the observational products used by *Deser et al.* [2010a], the tropical Pacific maximum is in disagreement with most of the observationally derived trends, some of which (HadISST1, Kaplanv2) suggest a cooling in the central/eastern equatorial Pacific. Whether this disagreement results from model deficiencies or can be attributed to the paucity of tropical observations is unclear. As discussed later in this section, the tropical maximum exhibited by climate models in their 21st century projections has been the subject of several studies [*Liu et al.*, 2005; *Di Nezio et al.*, 2009; *Xie et al.*, 2010]. The 20th century trends have large differences across models (not shown), both in terms of patterns and intensity. Figure 3 (bottom) shows the spread of the modeled trends. The spread can result from both model error and internal variability, as shown by *Deser et al.* [2010b]. The largest disagreement among models is found in the North Atlantic, north of 45°N, including the area where the model ensemble average shows cooling, as well as in the Bering Sea, Barents Sea, and in the Kuroshio Extension.

[23] The ensemble mean epoch difference fields (Period2, 2050–2099 minus Period1, 1950–1999) for SST according to the SRES-A2 scenario, is shown in Figure 4a. The ensemble mean SST difference is significant over most of the ocean, with agreement among models on the sign of the change. Exceptions are portions of the North Atlantic and the Southern Ocean, where there is model disagreement. At 200 m, statistical significance and model agreement are found in the subtropical gyres, most of the Tropics, and Southern Ocean (Figure 4b). Notice how the patterns of warming at the surface and 200 m differ. In the tropical Pacific, at 200 m warming is limited to the eastern half of the basin, while a weak cooling is present in the western equatorial Pacific, likely associated with a shoaling of the thermocline [*Han et al.*, 2006].

[24] The general pattern of surface warming (Figure 4a) has strong similarities with the 20th century trend in Figure 3 (top). In particular, SSTs are enhanced in the equatorial band, especially in the Pacific, with maximum values of ~2.4°C. This is the enhanced equatorial response (EER) pattern described by *Liu et al.* [2005], and further investigated by *Xie et al.* [2010] in the GFDL-CM2.1 model. In that model, reduced SST damping along the equator associated with the mean evaporation pattern appears to be responsible for the enhanced warming. The dominant role of air-sea interactions for the EER is consistent with the absence of the enhanced equatorial warming at 200 m (Figure 4b). Temperature increases of ~2°C are also seen in the Southern Ocean, along the 30°–45°S band, especially in the Indian and Pacific sectors, consistent with the 20th century trend. A temperature increase of up to 3°C is seen close to the southern tip of Australia, also consistent with the 20th century trend in both the model ensemble average and observations. Large SST changes, up to ~3.5°C, are found in the Barents Sea and along the Kuroshio Extension in the North Pacific.

[25] The pattern of SST increase is qualitatively similar to that described by *Xie et al.* [2010, Figure 2] for the GFDL-CM2.1 model considering the SRES-A1B scenario. A noticeable feature of the pattern in Figure 4a, also discussed by both *Liu et al.* [2005] and *Xie et al.* [2010] is the larger warming in the Northern Hemisphere relative to the

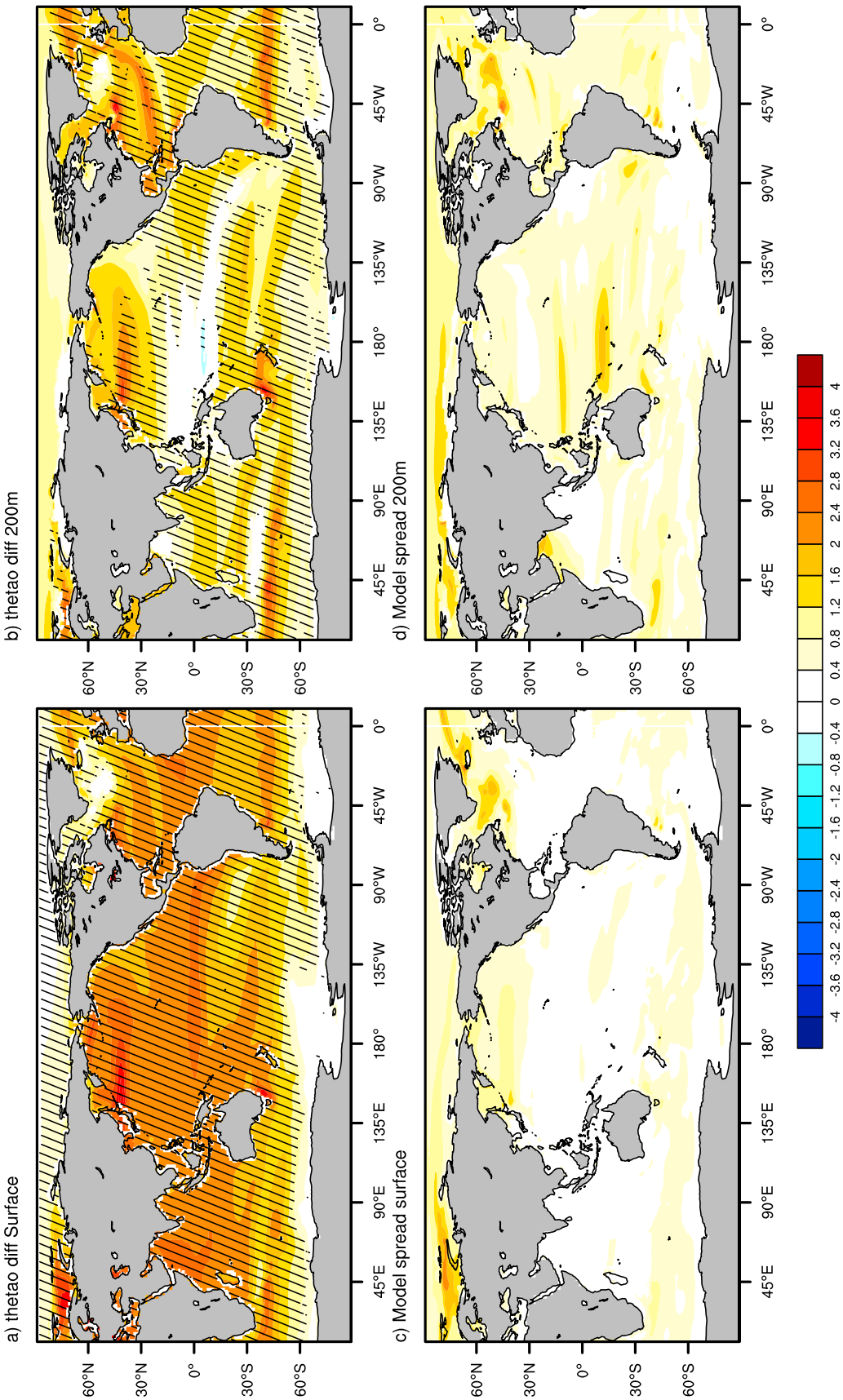

Figure 4. Multimodel ensemble average of temperature differences (Period2-Period1) at (a) the surface and (b) 200 m. The multimodel standard deviations at (c) the surface and (d) 200 m are also shown. As explained in section 2, hatching in Figures 4a and 4b indicates that the differences are statistically significant at the 95% level in at least 50% of the models, and 80% of the models agree on the sign of the change. Shading with no hatching indicates that the temperature changes are within the level of internal variability. White areas in Figures 4a and 4b correspond to areas where differences are smaller than 0.4 (our contour interval) or changes are significant, but less than 80% of the models agree on the sign of the change.

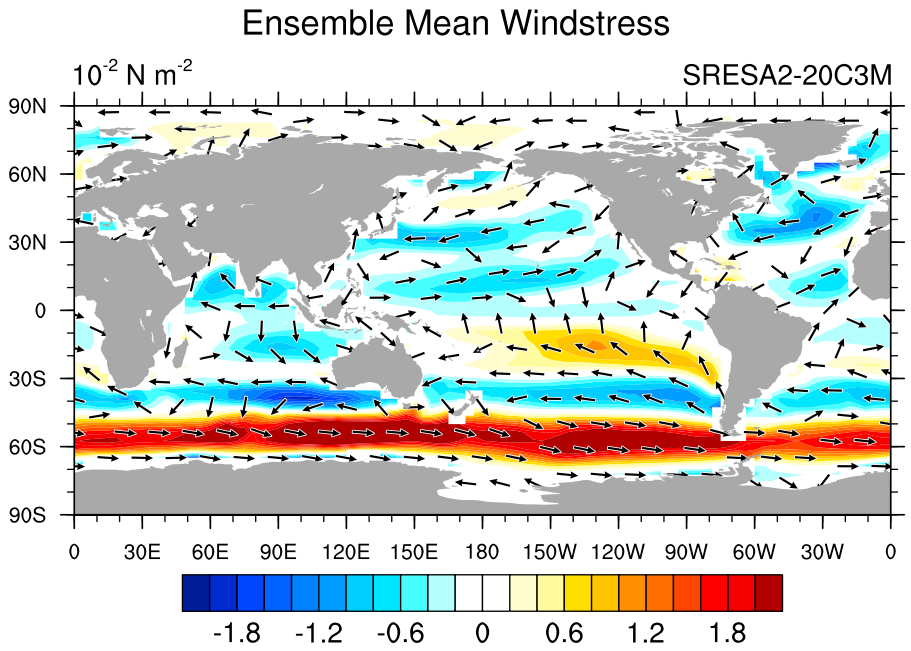

Figure 5. Multimodel ensemble average of the surface wind stress difference between Period2 and Period1. Arrows show the wind stress changes, shading shows differences in magnitude.

Southern Hemisphere. The main reason for this hemispheric asymmetry is associated with the changes in wind stress, which weakens in the northern subtropics and midlatitudes, but strengthens in the Southern Hemisphere subtropics in the Pacific, and, to a lesser degree, Atlantic sectors (Figure 5). In particular, the tongue of reduced warming that extends northwestward from the west coast of southern South America (Figure 4a) coincides with an area of strong enhancement of the Southern Hemisphere trade winds. Figure 5 also shows large changes in the Southern Ocean midlatitude westerlies, which shift poleward and intensify, as discussed by previous studies [*Sen Gupta et al.*, 2009, and references therein]. The stronger westerlies along roughly 60°S are accompanied by enhanced equatorward Ekman transports, which serve to mitigate the warming. In the North Atlantic, the pattern of warming is characterized by banded structures extending northeastward from the Caribbean. These structures have also been noticed by *Xie et al.* [2010], and attributed to ocean dynamics.

[26] Figure 4c shows the multimodel standard deviation of SST differences, a measure of the differences among models and uncertainty in the SST change projections. The largest differences among models are found in the Arctic Ocean, especially the Barents Sea, as well as in the North Atlantic, North Pacific, and Southern Ocean. Differences in ice cover may be partly responsible for the different SST changes in the Arctic, while inter-model differences in the position of the Gulf Stream and Kuroshio, as well as their projected changes, may give rise to local differences in SST change in the North Atlantic and North Pacific. Figure 4c also shows the presence of inter-model differences in SST change of the order of ~0.5°–0.75°C over the Southern Ocean. The degree of warming south of 45°S appears to be related to the degree of intensification of the midlatitude westerlies in each model, as shown in Figure 6, where the average warming in the 50°–60°S circumpolar belt is plotted against the changes in wind speed averaged over the same area. The models with stronger westerlies in the second half of the 21st century show modest warming, while models with

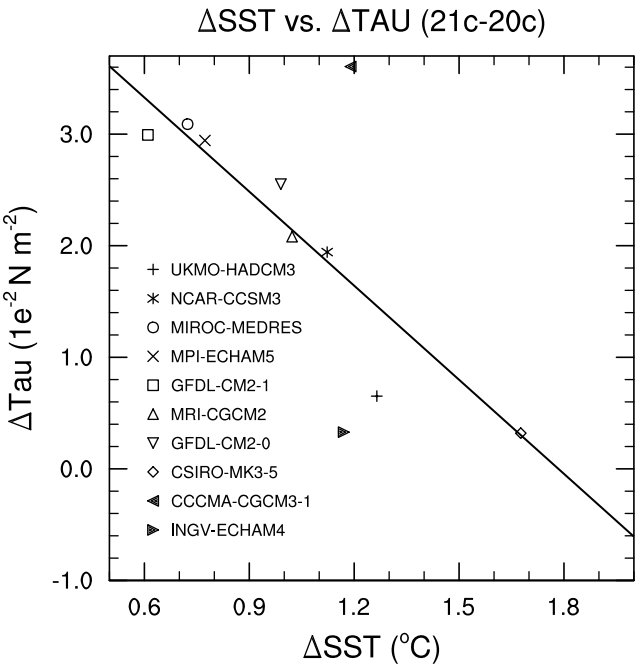

Figure 6. Changes in the amplitude of the surface wind stress over the circumpolar belt between 50°S and 60°S versus changes in SST averaged over the same region. The 50°S–60°S circumpolar band is the area in the Southern Ocean with the largest intensification of westerlies in the multimodel mean (Figure 5). The correlation coefficient between wind stress and SST changes is −0.71, which is significant at the 97.5% level.

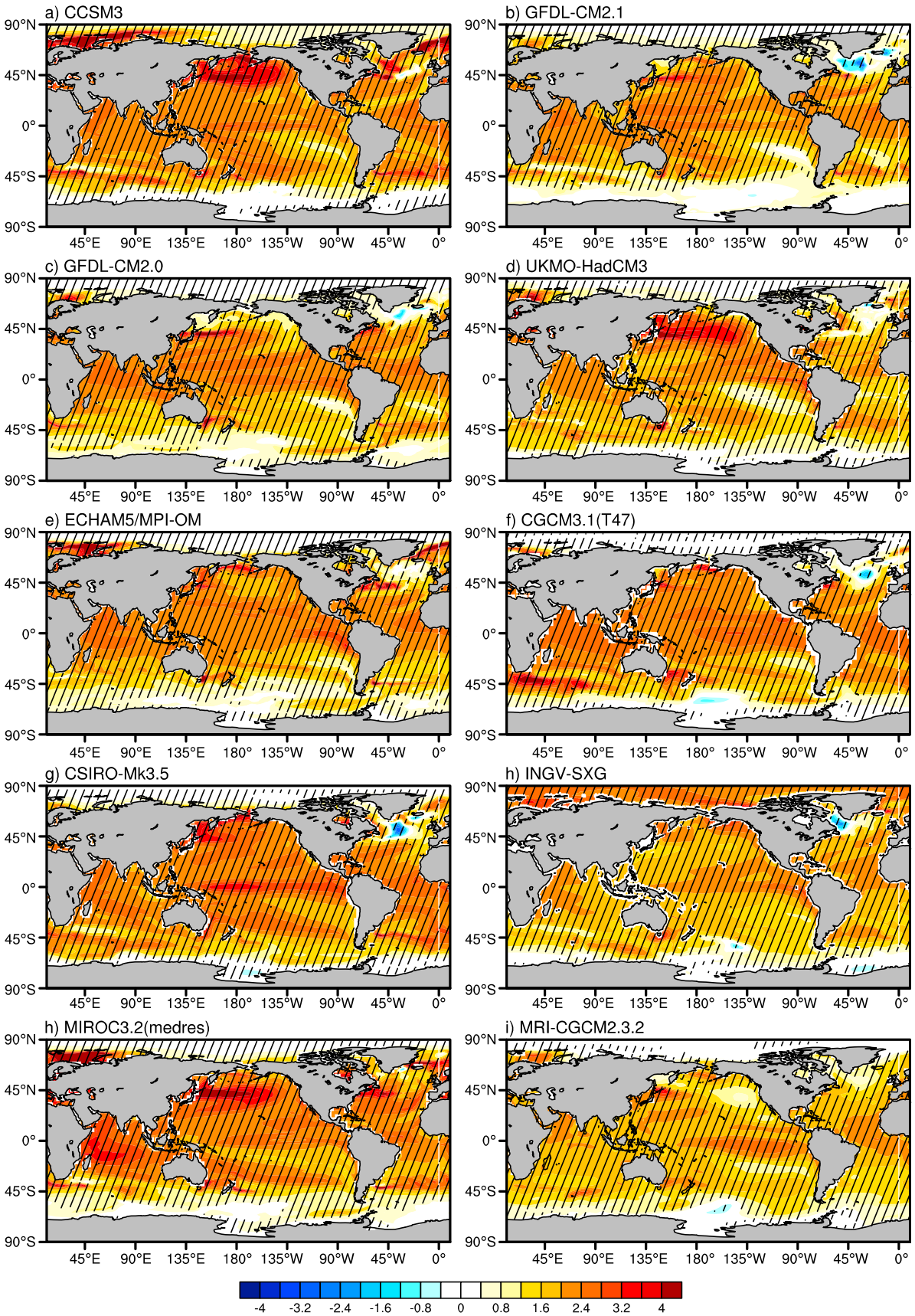

Figure 7. SST differences (Period2-Period1) for the ten individual models. Hatching indicates statistical significance at the 95% level.

small changes in their circumpolar winds tend to warm more. The poleward strengthening of the circumpolar winds is due to both increase in the greenhouse gases and ozone depletion, and varies among models depending on the degree of ozone recovery prescribed in each model [*Son et al.*, 2008].

[27] At 200 m, the largest discrepancies among models are also found in the Arctic, North Atlantic, as well as along tropical zonal bands around 10°–15° from the equator. Comparison with Figure 4b indicates that while the spread in the Arctic is associated with natural variability, the model spread in the North Atlantic and Tropics correspond to statistically significant changes of different sign in different models. In the Tropics, temperature changes at a fixed depth are likely associated with vertical displacements of the mean isotherms. The mean structure of the thermocline as well as the position of the mean tropical currents may vary from model to model.

[28] To illustrate the range of uncertainty in the SST changes, Figure 7 shows the SST epoch differences (Period2-Period1) for all the ten models. The equatorial warming in the Pacific ranges from 2°–2.4°C (INGV-SXG) to ∼3.5°C (CSIRO-Mk3.5), with a pattern that is either eastward intensified (UKMO-HadCM3, ECHAM5/MPI-CM, CGCM3.1 (T47), INGV-SXG, MRI-CGCM2.3.2), westward intensified (GFDL-CM2.1), or quasi-uniform along the equator (CCSM3, GFDL-CM2.0, CSIRO-Mk3.5, MIROC3.2(medres)). Large differences among models are also found in the North Pacific, where some models show extensive warming up to 4°C (CCSM3, UKMO-HadCM3, MIROC3.2(medres)), while other models, INGV-SXG being the extreme case, show only moderate warming. In the North Atlantic, with the exception of MIROC3.2(medres), all models show areas of negligible warming or cooling, but there are differences in the exact location of those areas. In the Arctic Ocean, the INGV-SXG shows extensive warming over the whole Arctic, while for the rest of the models the warming is limited to the Barents Sea, with varying magnitudes.

4. Changes in the Salinity Field

[29] Figure 8a shows the ensemble average of the mean evaporation minus precipitation (E-P) over the period 1950–1999. The large-scale pattern is in agreement with observational estimates over the period 1980–1993 [*Josey et al.*, 1998]. Precipitation exceeds evaporation in the tropics, especially over the western equatorial Pacific and eastern Indian Ocean, along the Pacific Intertropical Convergence Zone (ITCZ, 5°–7°N), and in the area of the South Pacific Convergence Zone (SPCZ), extending southeastward from the equator to ∼10°S. Enhanced precipitation is also found at high-latitudes, poleward of 45° in both hemispheres. Evaporation exceeds precipitation in the sub-tropics, especially in the eastern part of the basins in the Southern Hemisphere. The ensemble average projected changes in E-P (Figure 8b) have a spatial distribution that is very similar to the mean E-P field: precipitation, relative to evaporation, increases over the tropical regions and in high-latitudes, and decreases in the subtropics over the second half of the 21st century, an indication of a strengthened hydrological cycle [*Held and Soden*, 2006].

[30] These changes in the surface freshwater flux into the ocean can be expected to have a large impact upon salinity. *Durack and Wijffels* [2010] have used a large number of salinity profiles from historical archives and the International Argo Program to compute global multidecadal linear trends of ocean salinity. Before examining the changes in salinity over the second half of the 21st century, we compare the ensemble average mean salinity and salinity trend over the second half of the 20th century with those estimated by *Durack and Wijffels* [2010]. In contrast with SST, to first order there are no direct feedbacks between SSS and freshwater flux, so that salinity is weakly constrained by the surface forcing. In climate models, where the oceanic and atmospheric components interact freely, the surface salinity field may develop unrealistic features.

[31] Figure 9 compares the ensemble average mean salinity in 1950–2000 (Figure 9, bottom) with that computed by *Durack and Wijffels* [2010], and reproduced from their paper in Figure 9 (top), over the same period. Notice that the study of *Durack and Wijffels* [2010] does not include marginal seas. The polar regions were also not included in their analysis. Apart from the underestimate of the salinity values in the Southern Hemisphere subtropics, and the excessive freshening in the area of the SPCZ, the latter likely due to the models too intense and extensive SPCZ regions [*Lin*, 2007; *Bellucci et al.*, 2010], the model-derived SSS compares well with the observed both in pattern and magnitude. The models even reproduce the strong salinity contrast between the salty Arabic Sea and the fresh Bay of Bengal in the northern Indian Ocean. However, in spite of the good comparison of the multimodel mean, individual models may have large salinity biases in some regions (not shown). The mean salinity pattern from the models has a strong similarity with the mean E-P field shown in Figure 8a, so that areas with low SSS are approximately found in regions of negative E-P, and saltier regions tend to be co-located with regions of positive E-P, an indication of the controlling influence of the local surface forcing upon the SSS distribution. However, in some areas, like the northeast Pacific, low salinity waters extend all the way to the equator along the western coast of North America, in spite of the positive E-P south of 30°N. Southward advection of low salinity water by the California Current is likely responsible for the difference between SSS and local freshwater flux forcing along the western coast of North America, south of 30°N.

[32] The multimodel ensemble SSS trend during 1950–1999 is compared in Figure 10 with the observational estimate of *Durack and Wijffels* [2010]. The trend is overall weaker in the multimodel average (Figure 10b) than in observations, but the general pattern is consistent between the two products. Individual model's trends (not shown) are as large as those found in observations (Figure 10a), but trend patterns in different models are shifted in space, and are of different sign in some regions, so that the averaging procedure leads to some loss of signal. A similar reduction in amplitude associated with averaging across multiple model simulations was noted by *Knutti et al.* [2010] for precipitation. The major discrepancies between the multi model mean trend (Figure 10b) and the observational estimate of Durack and Wijffels (Figure 10a) are found in the North Pacific where the observed trend shows a large freshening across the whole basin while the model freshening trend is confined to the eastern half of the North Pacific, and in the North Atlantic, where the multimodel mean has a negative trend.

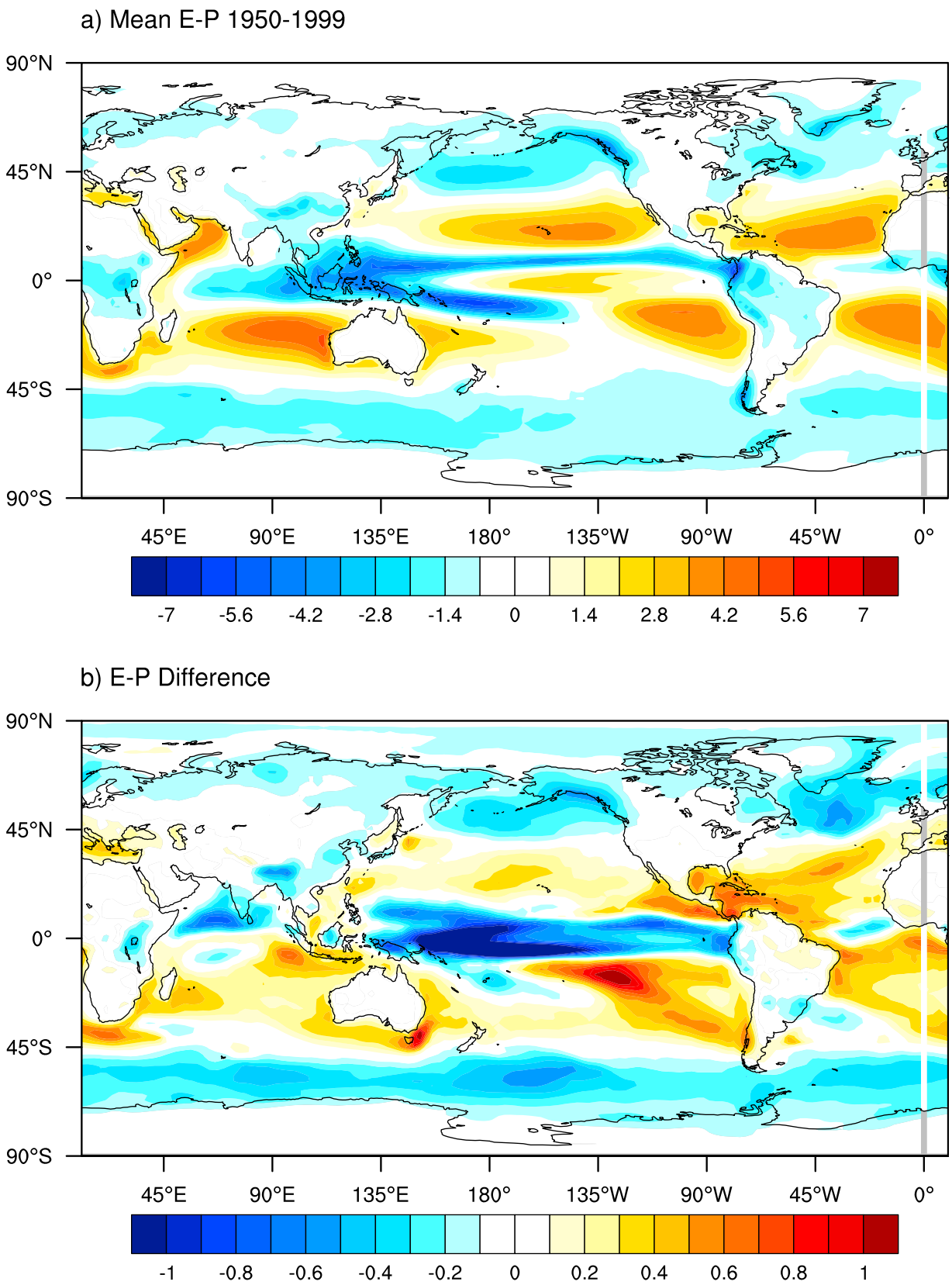

Figure 8. (a) Multimodel ensemble mean of evaporation (E) minus precipitation (P) averaged over 1950–1999. (b) Multimodel ensemble mean of the E-P difference (Period2-Period1). Units are mm/day.

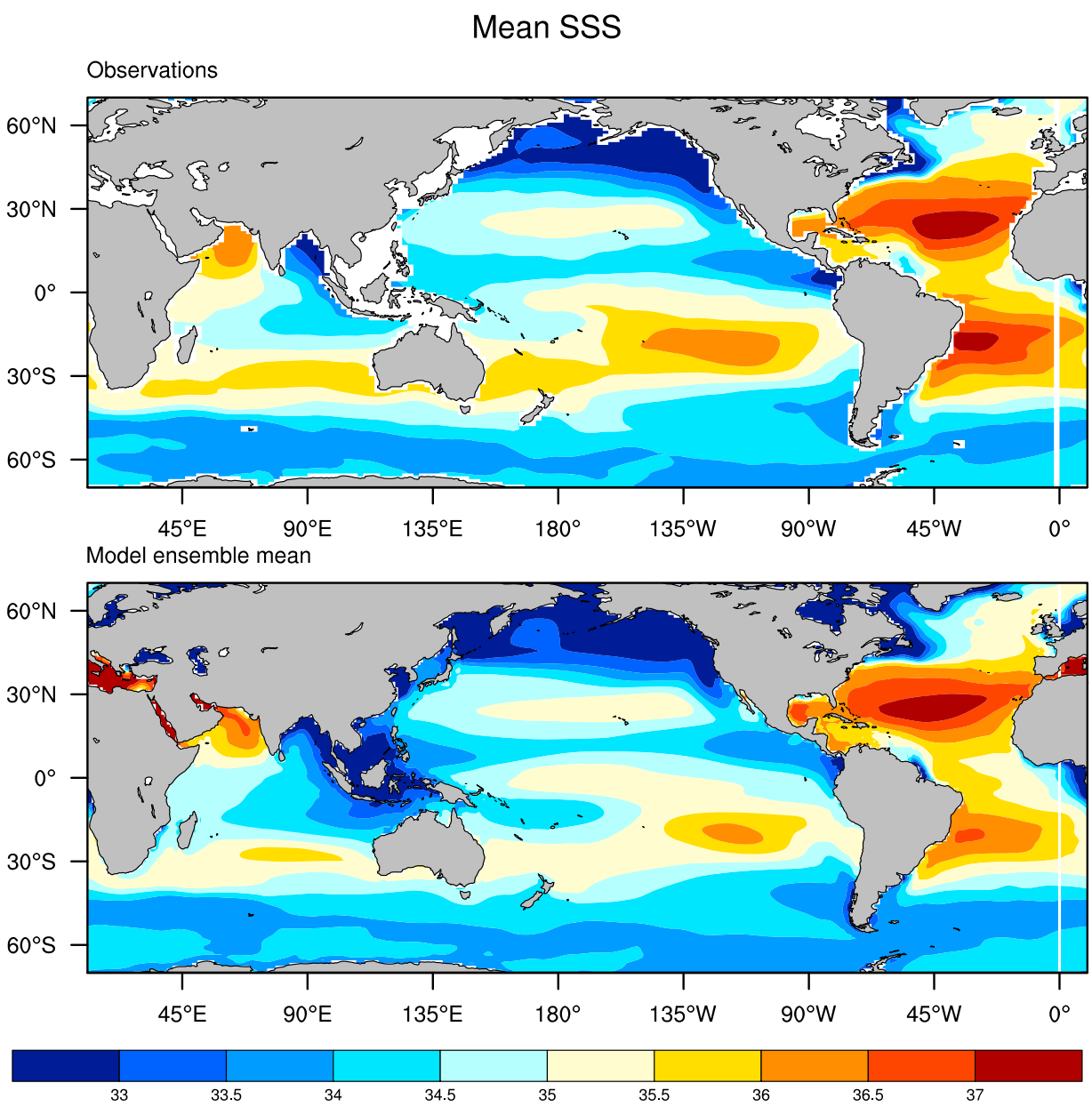

Figure 9. (top) Mean SSS (psu) computed from observations by *Durack and Wijffels* [2010], courtesy of P. Durack and S. Wijffels. (bottom) Multimodel ensemble average of mean SSS over the same period 1950–1999 from the 20th century simulations. Notice that the analysis of *Durack and Wijffels* [2010] does not include marginal seas.

The application of the statistical significance criteria described in section 2 to the multimodel 50-year trend (Figure 10c) shows that there are only few areas where the trend is statistically significant in 50% of the models and there is agreement in sign in at least 80% of the models. These areas include the northeast Pacific, the western tropical/subtropical North Atlantic and some regions of the Southern Ocean. On the other hand, there are large areas that are white in Figure 10c relative to Figure 10b (for example the North Atlantic north of ~45°N, and large parts of the northern and tropical Pacific), indicating model disagreement on the sign of a detectable trend signal, and thus large

Figure 10. (a) 50-year SSS linear trend (psu (50 yrs)$^{-1}$) over the period 1950–2000 computed from observations by *Durack and Wijffels* [2010], courtesy of P. Durack and S. Wijffels. (b) Multimodel ensemble average of SSS trend over 1950–1999 from the 20th century simulations. (c) Same as Figure 10b, but including statistical significance and robustness information, as described for Figure 4. The broad areas that are white in Figure 10c relative to Figure 10b identify regions of large uncertainty, as the trend signal is above the internal variability level in 50% of the models in those areas, but the models disagree on the sign of the trend.

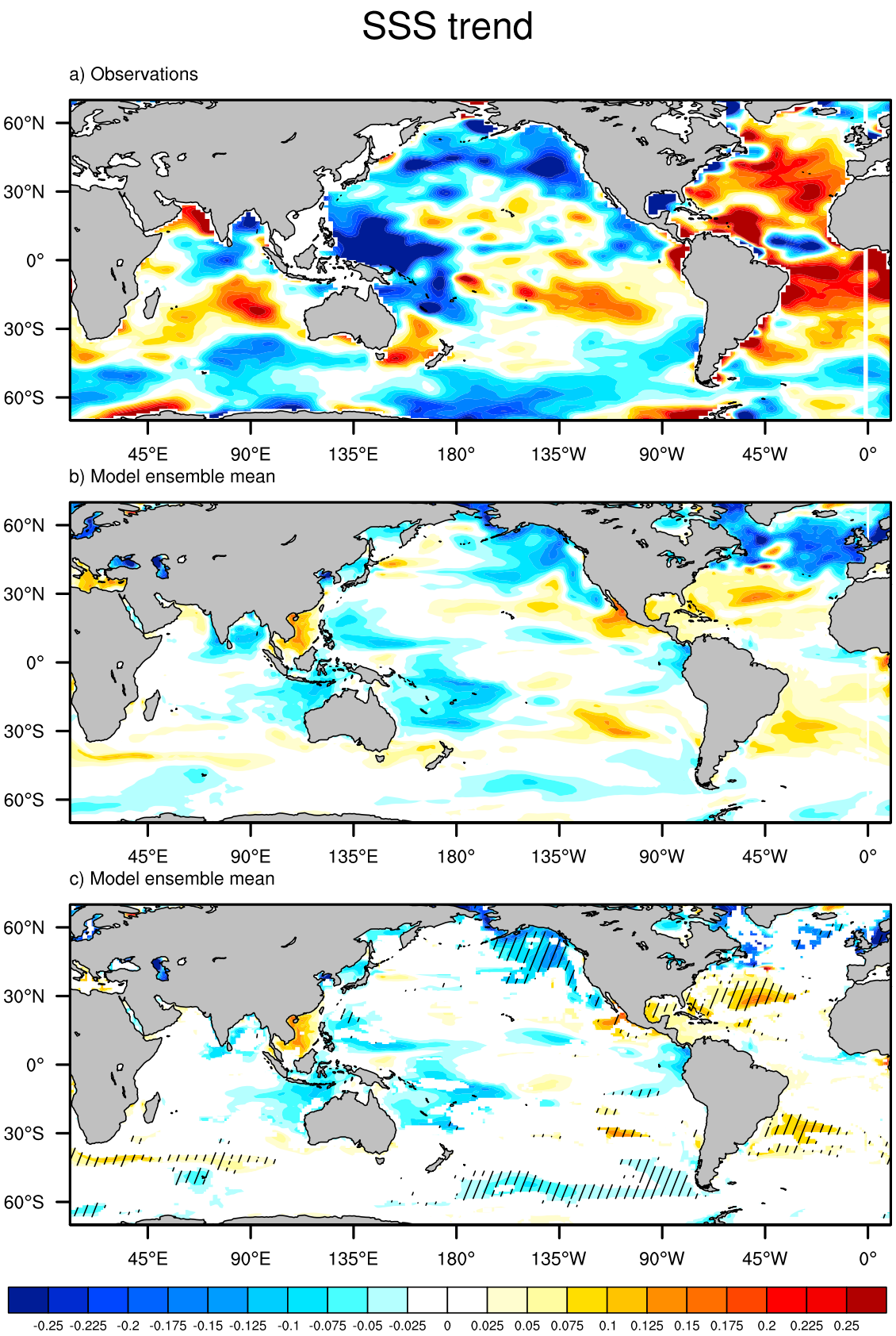
SSS trend
a) Observations
b) Model ensemble mean
c) Model ensemble mean
60°N
30°N
0°
30°S
60°S
45°E
90°E
135°E
180°
135°W
90°W
45°W
0°
-0.25 -0.225 -0.2 -0.175 -0.15 -0.125 -0.1 -0.075 -0.05 -0.025 0 0.025 0.05 0.075 0.1 0.125 0.15 0.175 0.2 0.225 0.25

Figure 10

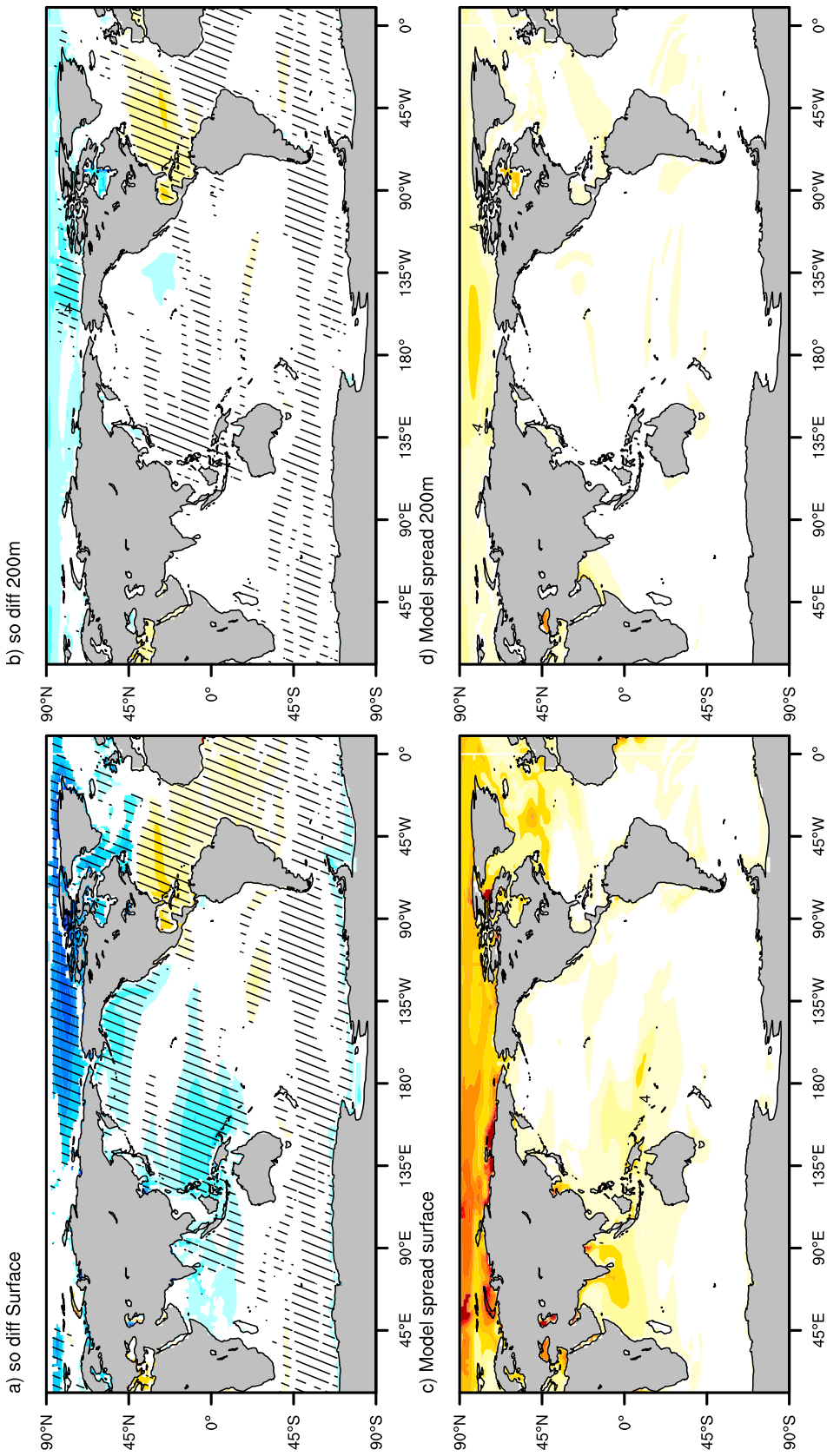

Figure 11. Multimodel ensemble average of salinity (psu) differences (Period2-Period1) at (a) the surface and (b) 200 m. The multimodel standard deviations at (c) the surface and (d) 200 m are also shown. The meaning of the hatched and white areas in Figures 11a and 11b is as described in Figure 4.

uncertainty in the models simulation of the trend over the second half of the 20th century.

[33] The change in the pattern of SSS between the second half of the 21st century and the second half of the 20th century (Figure 11a) is very similar to the trend seen in Figure 10b. Hatched and white areas have the same meaning as in Figure 4. The areas where the salinity changes are significant across models, and there is agreement in sign for eight of the models used, include the western tropical Pacific, northeast Pacific, part of the Arctic, Labrador Sea and part of the North Atlantic, as well as the tropical Atlantic. The signal in the Southern Ocean is small, except near the Antarctic Peninsula.

[34] Figure 11c shows that the models tend to disagree in their SSS projections in the western tropical Pacific, especially in the SPCZ area, in the Indian Ocean, as well as in the North Atlantic and Arctic. Comparison with Figure 11a suggests that in the western tropical Pacific, eastern half of the Indian Ocean, and in the Arctic east of ~150°E most models agree in sign, so that the model spread is an indication of differences in magnitude. On the other hand, between 45°E and 135°E in the Arctic, and in vast regions of the North Atlantic, there seem to be a large uncertainty also on the sign of the change.

[35] At 200 m, the largest salinity changes are the freshening of the Arctic, and the increased salinity in the subtropical North Atlantic and in the Mediterranean Sea (Figure 11b), changes that appear to be robust among models, as indicated by the hatching. The largest spread among models is found in the Arctic (Figure 11d). *Holland et al.* [2008] have shown that all the fourteen models considered in their study exhibit a decrease in sea ice volume during the 21st century, according to the SRES-A1B scenario, which is consistent with the overall freshening of the Arctic seen in Figure 11 (we expect the SREAS-A2 scenario to have qualitatively similar projections). However, the magnitude of sea ice loss, as well as the relative roles of changing melt and growth, varied considerably among models, and appeared to be dependent upon the initial ice climatology. The large spread in salinity projections in the Arctic may partly reflect the different ice loss in different models. Changes in precipitation and runoff can also play an important role in the Arctic salinity changes [*Rawlins et al.*, 2010]. Differences in precipitation projections, as well as in the specification of runoff in different models, may also be important factors in the large model spread of salinity projections over the Arctic.

[36] Figure 12 shows the SSS changes for individual models, to illustrate inter-model differences. While there is agreement on the large-scale patterns of SSS changes, the regional expression of those changes differ among models. For example, freshening in the western equatorial Pacific is confined to a relatively narrow meridional band in CCSM3 and MIROC3.2(medres), while in the rest of the models the freshening is of broader meridional extent. In particular, in UKMO-HadCM3 freshening is predominant over most of the north Pacific. MIROC3.2(medres) shows a large freshening in the Indian Ocean, which is absent in many of the other models. In the Arctic, there are areas where the models agree in sign, explaining the robustness seen in Figure 11a (hatched area), but large differences in sign and magnitude are seen west of ~135°E.

[37] While the surface freshwater flux has a large impact on the salinity field locally, the salinity changes are not completely determined by the surface fluxes. Figure 13 compares the changes in SSS (Figures 13b and 13d, repeated from Figure 12) with the changes in the surface freshwater flux (Figures 13a and 13c) for two models, the UKMO-HadCM3 and the NCAR-CCSM3. Among the models examined in this study, the UKMO-HadCM3 is one with extensive North Pacific freshening. Apart from a narrow band in the vicinity of the Kuroshio Extension, salinity decreases over the entire North Pacific, even in the subtropics, where the changes in E-P are positive. In the NCAR-CCSM3 the SSS changes tend to be more closely co-located with the freshwater flux changes. However, there are areas, like the northeast Pacific, where decreased SSS is found along the western coast of North America all the way to Baja California, in spite of the positive E-P change south of ~35°N. As already noted for the mean salinity field, this is likely the result of southward advection of low-salinity waters by the California Current.

5. Density and Stratification Changes

[38] Not all the models used in this study have potential density available in the PCMDI archive. Density can be computed from temperature (T) and salinity (S) through the equation of state. Due to the nonlinearity of the equation of state, errors can arise when the equation is applied to monthly mean temperature and salinity fields. Here we use the McDougall, Wright, Jackett, and Feistel (MWJF) [*McDougall et al.*, 2003] polynomial approximation to compute density from T and S. To test the accuracy of the density values computed using the equation of state, for some of the models that provide density output we have compared the surface density changes computed directly from the density fields with the changes computed from time averages of T and S using the equation of state. Apart from the Arctic, and very localized areas in the northwest Atlantic and northwest Pacific, errors are very small. Thus, for consistency, we compute density using the equation of state for all the models.

[39] Density changes are estimated as

$$\Delta\rho = \rho(\overline{T}_2, \overline{S}_2) - \rho(\overline{T}_1, \overline{S}_1), \tag{1}$$

where overbars indicate time average quantities, $\overline{T}_1$ and $\overline{T}_2$ are the average temperature and salinity fields during Period1 (1950–1999), while $\overline{T}_2$ and $\overline{S}_2$ are the average T and S conditions during Period2 (2050–2099). The relative influence of the temperature and salinity changes upon the density changes is then estimated as

$$\Delta\rho_T = \rho(\overline{T}_2, \overline{S}_1) - \rho(\overline{T}_1, \overline{S}_1), \tag{2}$$

$$\Delta\rho_S = \rho(\overline{T}_1, \overline{S}_2) - \rho(\overline{T}_1, \overline{S}_1), \tag{3}$$

with $\Delta\rho_T$ and $\Delta\rho_S$ being the density changes due to the T and S changes, respectively. The approach outlined in equations (2) and (3) is not exact, as the sum of $\Delta\rho_T$ and $\Delta\rho_S$ does not exactly match $\Delta\rho$, but the discrepancies are very small, so that (2) and (3) provide a good estimate of the T and S contributions to the density changes. Figures 14a

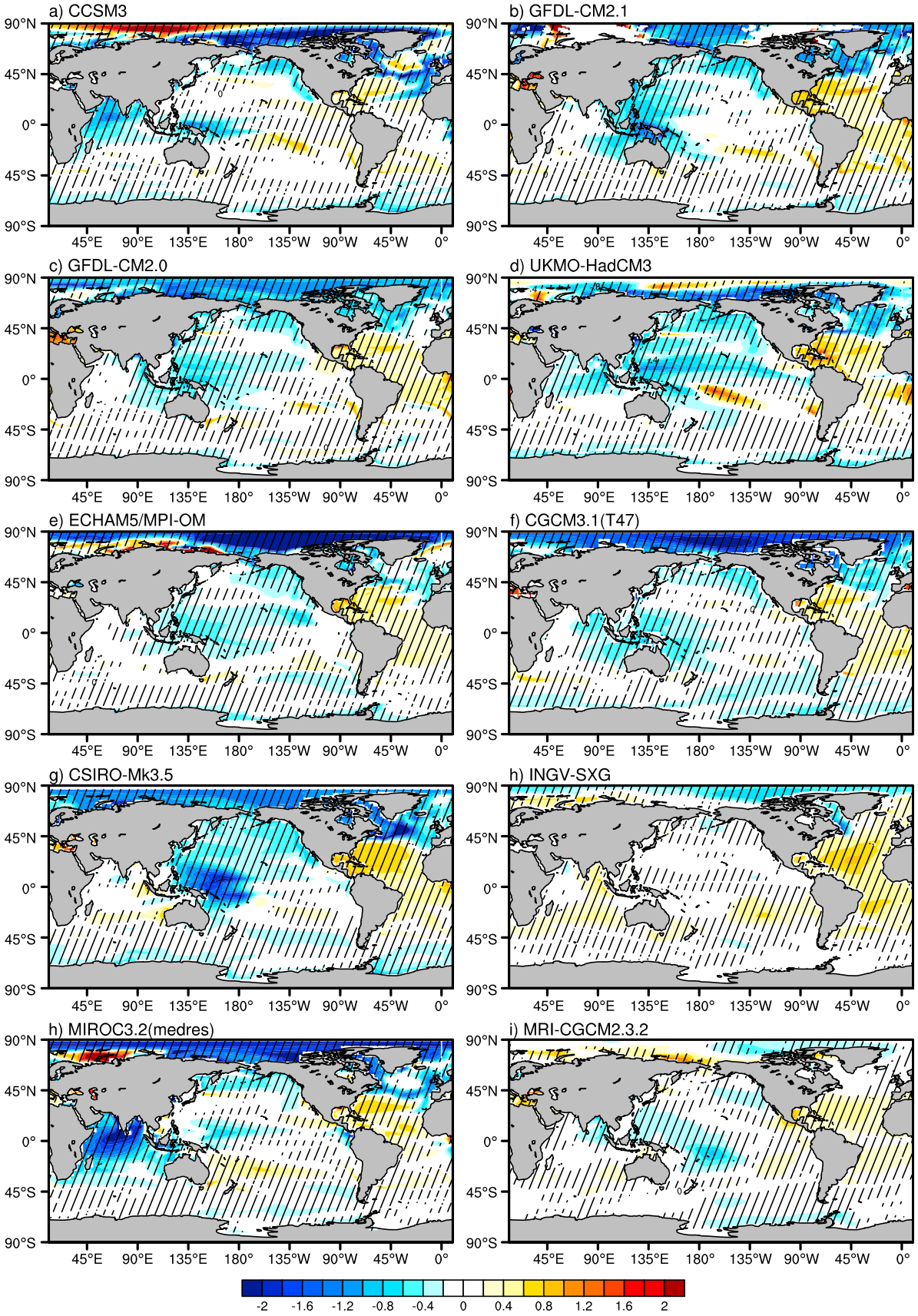

Figure 12. SSS difference for all ten models. Hatching indicates statistical significance at the 95% level.

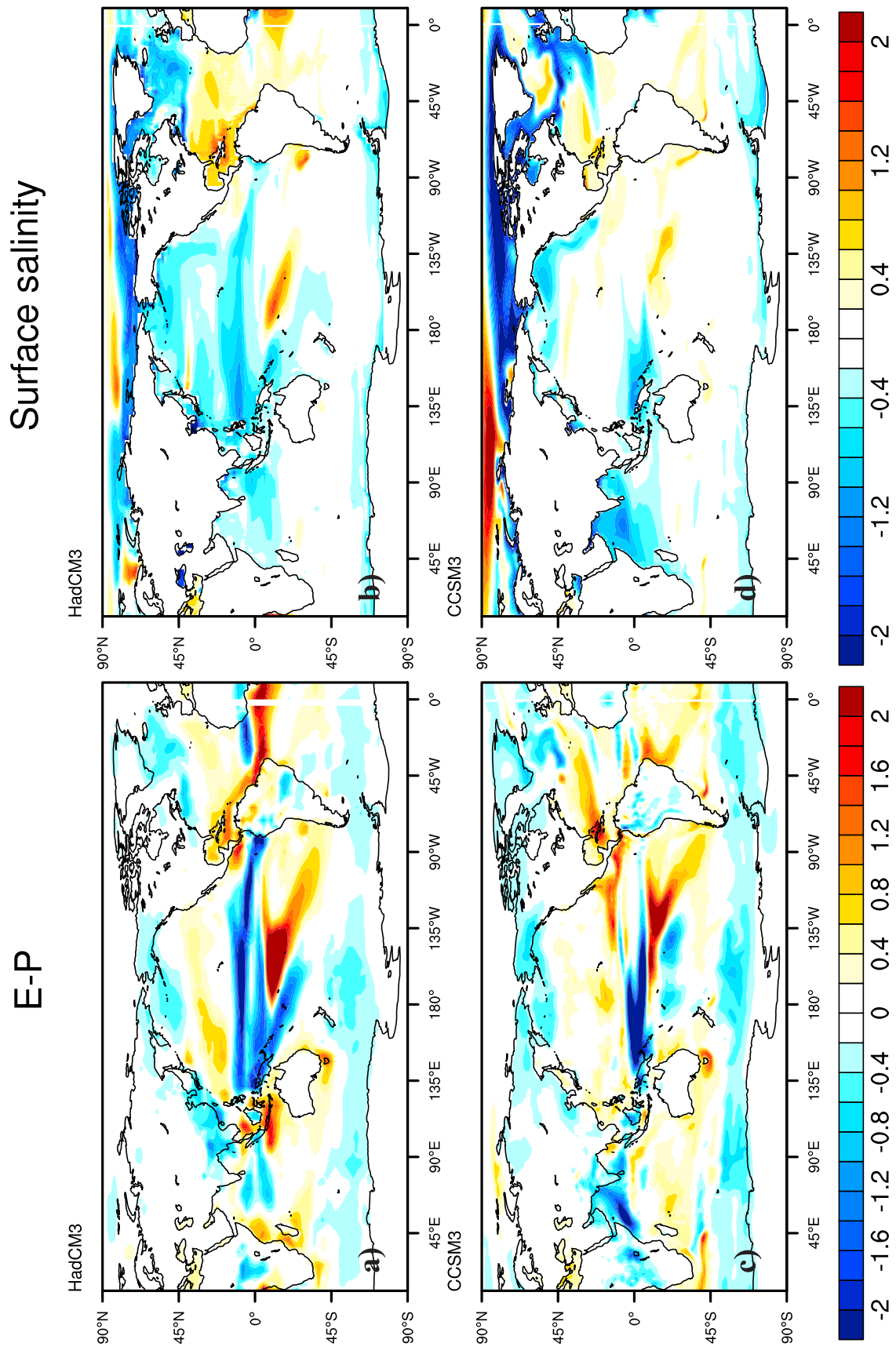

Figure 13. (a and c) Differences (Period2-Period1) of E-P (mm per day) and (b and d) SSS (psu) in UKMO-HadCM3 (Figures 13a and 13b) and CCSM3 (Figures 13c and 13d).

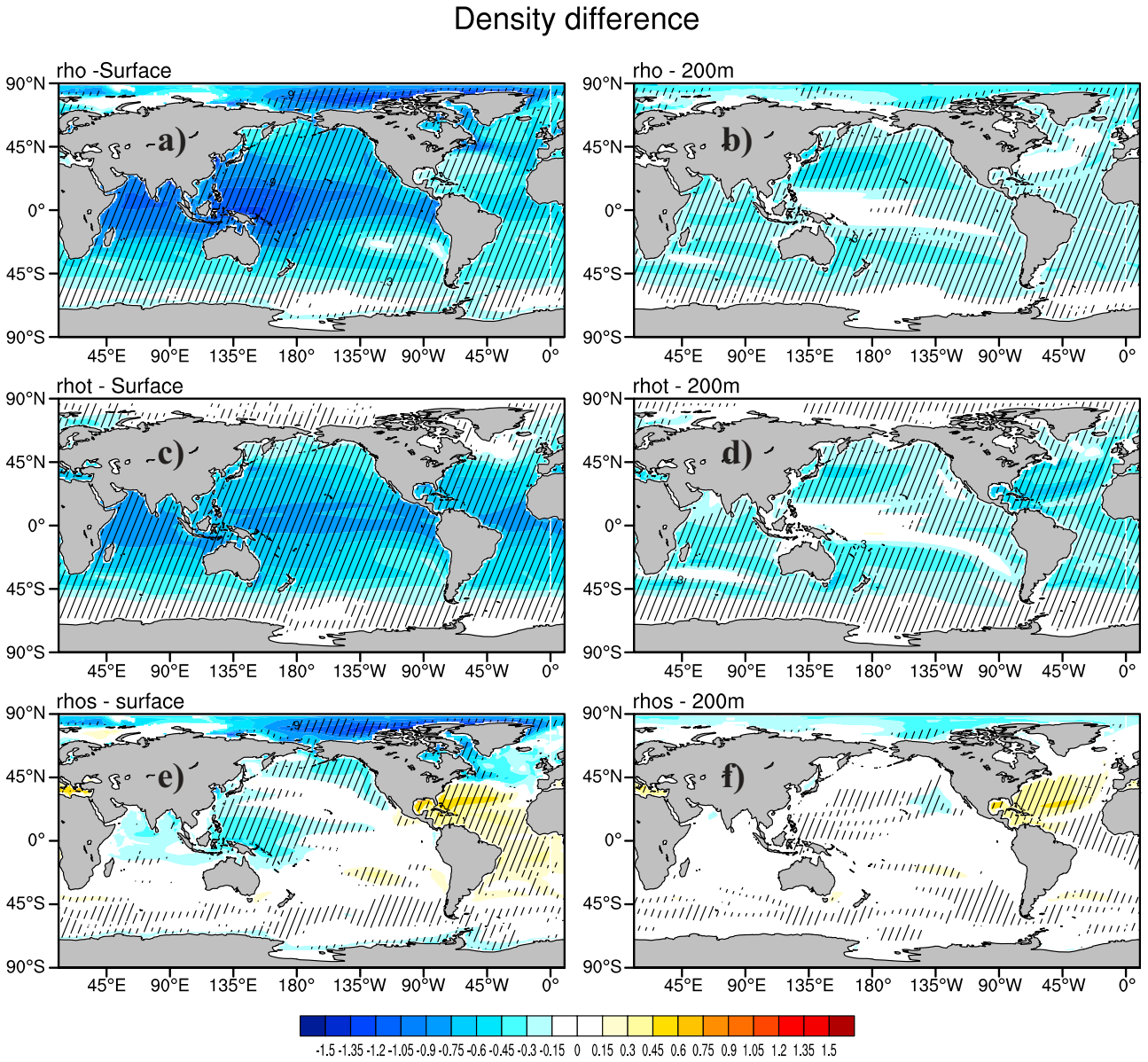

Figure 14. (a and b) Multimodel ensemble average of potential density (σ_θ units) differences (Period2-Period1) at the surface (Figures 14a, 14c, and 14e) and 200 m (Figures 14b, 14d, and 14f). The contribution of the (c and d) temperature and (e and f) salinity changes to the density changes are also shown. Hatching indicates areas where at least nine of the 10 models agree on the sign of the density change, while white areas are either areas where changes are smaller than the contour interval in absolute value, or where less than six models agree on the sign of the change.

and 14b show the ensemble average density change at the surface (Figure 14a) and at 200 m (Figure 14b). Due to the approach chosen to compute density (equations (1)–(3)), we cannot estimate the statistical significance of the density change for each model (which requires the evaluation of the amplitude of natural variability in periods 1 and 2). Thus, we resort to a measure of robustness, and indicate the degree of models' agreement on the sign of the density changes. Hatching is used when 90% of the models agree on the sign, while areas with less than 60% agreement are left white. At the surface, the density changes are particularly pronounced in the tropical Indo-Pacific sector and in the Arctic, while at

Figure 15. (top) Multimodel ensemble average of stratification changes (Period2-Period1), (middle) temperature contribution, and (bottom) salinity contribution. Stratification is defined as the density difference between 200 m and the surface. Hatching identifies areas where at least 90% of the models agree on the sign of the change. White areas correspond to regions where changes are below the contour interval in absolute value or less than 60% of the models agree on the sign of the change.

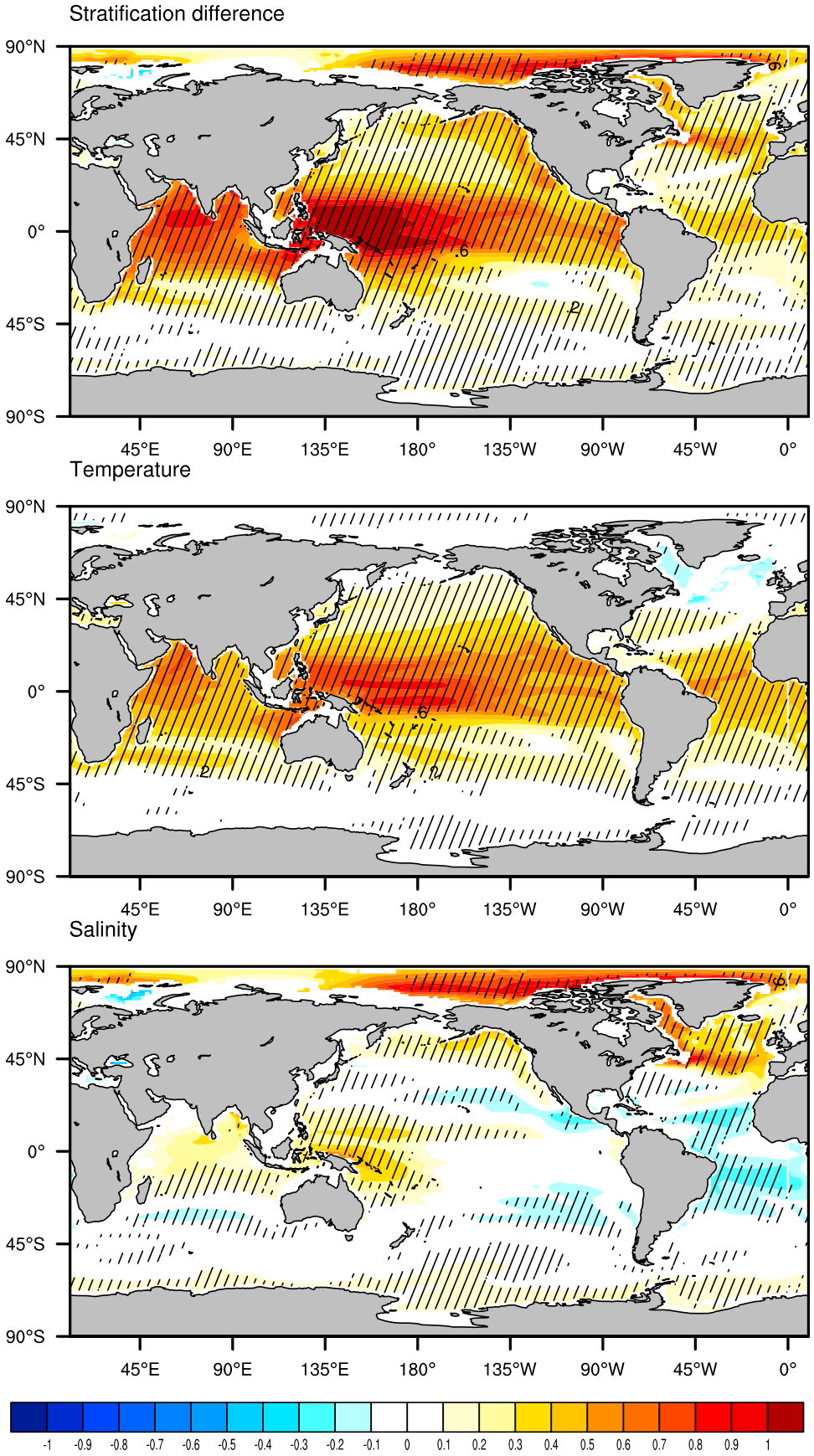
Stratification difference
90°N
45°N
0°
45°S
90°S
45°E
90°E
135°E
180°
135°W
90°W
45°W
0°
Temperature
Salinity
-1
-0.9
-0.8
-0.7
-0.6
-0.5
-0.4
-0.3
-0.2
-0.1
0
0.1
0.2
0.3
0.4
0.5
0.6
0.7
0.8
0.9
1

Figure 15

200 m the largest decreases are found in the subtropical gyres of the Pacific Ocean. In most regions, the temperature change is the major contributor to the density change (Figures 14c and 14d), favoring a density decrease everywhere, its influence decreasing with increasing latitude. The influence of salinity is more spatially limited, but can have large regional contributions to the density changes (Figures 14e and 14f). At the surface, salinity dominates the density changes in the Arctic east of the dateline, and portions of the North Atlantic and northeast Pacific, and contributes to the density decrease in the western tropical Pacific. Both at the surface and at 200 m, the salinity increase in the western tropical Atlantic counteracts the influence of the warming and reduces the density change in that area.

[40] Changes in stratification are computed as the differences between 200 m and surface density changes. Results for the multimodel ensemble are shown in Figure 15, where hatching and white shading are used as in Figure 14. Apart from the small area of the Arctic around 45°E, 80°N, where a hint of decreased stratification can be seen, stratification changes are positive everywhere. As indicated by the hatching, stratification changes are robust in most of the North Pacific, North Atlantic, Indian Ocean, as well as in the Arctic Ocean east of ∼135°E. Temperature is the major contributor to the stratification changes in the tropical and sub-tropical regions (Figure 15, middle), while salinity dominates the changes in the Arctic, northeast Pacific and North Atlantic (Figure 15, bottom), and also enhances the stratification increase in the western tropical Pacific and counteracts the warming in the tropical Atlantic.

6. Summary and Conclusions

[41] In this study we have documented the changes in upper ocean stratification projected by ten of the climate models participating in the Climate Model Intercomparison Project version 3. The changes have been computed as the difference between the mean conditions during 2050–2099, according to the SRES-A2 scenario, and the mean conditions in 1950–1999. Different aspects of the upper ocean density structure are important for ocean biogeochemical processes. Here we focus upon the density difference between the surface and 200 m, as indicative of the degree of coupling between the upper ocean mixed layer and the deeper ocean. The increase in stratification results from the large decrease in surface density, which, in turn, is a consequence of the SST and SSS changes. To provide a measure of statistical significance of our multimodel mean results we have first estimated the statistical significance of the SST and SSS changes in each models, to detect whether the climate change signal could be isolated from the model natural variability background, and then, for the areas where a signal could be detected in at least 50% of the models, we have examined the agreement on the sign of the change among models [*Tebaldi et al.*, 2011].

[42] The models used for this study differ in their projections at the regional scale. However, when a global perspective is adopted, patterns of broad-scale change emerge that are robust among models. Extensive stratification increases which meet the criteria of statistical significance and robustness adopted in this study for the temperature and salinity projections can be expected in the western tropical Pacific, Arctic Ocean east of ∼135°E, tropical Atlantic, northeast Pacific, and part of the North Atlantic.

[43] While temperature increases everywhere in the models, with the largest values in the tropics and along the Kuroshio Extension, the changes in sea surface salinity partly reflect the changes in the surface freshwater flux, which is characterized by increased precipitation over evaporation in the tropics and high-latitudes, and reduced precipitation in the sub-tropics. The salinity changes are also influenced by oceanic advection, leading, in some models, to freshening in areas where the changes in the net freshwater flux into the ocean are negative. Most models, and the multimodel mean, project an increased salinity contrast between the tropical Pacific and Atlantic oceans, with the tropical Pacific becoming fresher, and the tropical Atlantic saltier.

[44] Temperature changes are the largest contributor to the density and stratification changes at the broad scale. The temperature influence is largest in the tropical regions, and decreases with latitude. Salinity, on the other hand, appears to have a large regional influence, dominating the density and stratification changes in the Arctic, northeast Pacific and North Atlantic, and significantly contributing in the western tropical Pacific and tropical Atlantic.

[45] What are the possible consequences of the increased ocean stratification? The density jump at the base of the mixed layer has a direct impact upon entrainment, the process responsible for mixed layer deepening and for bringing nutrient-rich deep waters into the euphotic zone, where photosynthesis occurs. While other processes (mesoscale eddies, tropical and extra-tropical cyclones, atmospheric transport) may also play a key role in supplying nutrient to the euphotic zone, in most areas of the World Ocean nutrient availability for primary production relies upon entrainment processes. Some of the areas where the largest stratification changes occur, the Gulf of Alaska, California Current System, Northwest Atlantic, and along the subtropical front in the Southern Ocean, coincide with some of the most productive areas of the World Ocean (see maps of primary production at http://www.science.oregonstate.edu/ocean.productivity/). Thus, the projected stratification changes could have a large impact on phytoplankton and the broader food web. The effects of such changes may have already begun happening in sub-tropical waters [*Polovina et al.*, 2008]. Moreover, in four climate models that include representations of marine ecosystems and carbon cycle, a decrease in global mean primary productivity is found that approaches 20% by the end of the 21st century relative to pre-industrial conditions [*Steinacher et al.*, 2010]. The increase in upper ocean stratification can also impact the ventilation processes. For example, Mode Waters are projected to form on lighter isopycnal surfaces, and their volume is expected to be significantly reduced in the 21st century, based on the CMIP3 models simulations [*Luo and Rothstein*, 2009]. The declining trend of oceanic oxygen concentration observed in several areas is also attributed to stratification changes, but it is a non-local problem [e.g., *Bograd et al.*, 2008]. Further studies are needed to examine the characteristics of ocean ventilation in a warmer climate.

[46] **Acknowledgments.** We acknowledge the modeling groups, the Program for Climate Model Diagnosis and Intercomparison (PCMDI) and

the WCRP's Working Group on Coupled Modeling (WGCM) for their roles in making available the WCRP CMIP3 multimodel data set. Support of this data set is provided by the Office of Science, U.S. Department of Energy. We thank C. Deser and W. Large for very insightful suggestions at an early stage of this study, and P. Durack and S. Wijffels for making their salinity data available to us. Claudia Tebaldi has provided invaluable help with the statistical significance computation. We also thank A. Sen Gupta, and P. Durack for their excellent comments on earlier versions of the manuscript. Support for this study was provided by NSF grant 1544901 as part of the synthesis phase of the GLOBEC Program.

References

Allen, M. R., and W. J. Ingram (2002), Constraints on future changes in climate and the hydrological cycle, *Nature*, *419*, 224–232, doi:10.1038/nature01092.

Alley, R. B., et al. (2007), Summary for policymakers, in *Climate Change 2007: The Physical Science Basis: Working Group I Contribution to the Fourth Assessment Report of the Intergovernmental Panel on Climate Change*, edtied by S. Solomon et al., pp. 1–18, Cambridge Univ. Press, New York.

Bellucci, A., S. Gualdi, and A. Navarra (2010), The double-ITCZ syndrome in coupled general circulation models: The role of large-scale vertical circulation regimes, *J. Clim.*, *23*, 1127–1145, doi:10.1175/2009JCLI3002.1.

Bograd, S. J., C. G. Castro, E. Di Lorenzo, D. M. Palacios, H. Bailey, W. Gilly, and F. P. Chavez (2008), Oxygen declines and the shoaling of the hypoxic boundary in the California Current, *Geophys. Res. Lett.*, *35*, L12607, doi:10.1029/2008GL034185.

Cai, W., and H. B. Gordon (1999), Southern high-latitude ocean climate drift in a coupled model, *J. Clim.*, *12*, 132–146, doi:10.1175/1520-0442-12.1.132.

Clifford, M. A. (1983), A descriptive study of the zonation of the Antarctic Circumpolar Current and its relation to wind stress and ice cover, M.Sc. thesis, 93 pp., Tex. A&M Univ., College Station, Tex.

Collins, W. D., et al. (2006), The Community Climate System Model Version 3 (CCSM3), *J. Clim.*, *19*, 2122–2143, doi:10.1175/JCLI3761.1.

Covey, C., P. J. Gleckler, T. J. Phillips, and D. C. Bader (2006), Secular trends and climate drift in coupled ocean-atmosphere general circulation models, *J. Geophys. Res.*, *111*, D03107, doi:10.1029/2005JD006009.

Cravatte, S., T. Delcroix, D. Zhang, M. J. McPhaden, and J. Leloup (2009), Observed freshening and warming of the western Pacific Warm Pool, *Clim. Dyn.*, *33*, 565–589, doi:10.1007/s00382-009-0526-7.

Delworth, T. L., et al. (2006), GFDL's CM2 global coupled climate models. Part I: Formulation and simulation characteristics, *J. Clim.*, *19*, 643–674, doi:10.1175/JCLI3629.1.

Deser, C., A. S. Phillips, and M. A. Alexander (2010a), Twentieth century tropical sea surface temperature trends revisited, *Geophys. Res. Lett.*, *37*, L10701, doi:10.1029/2010GL043321.

Deser, C., A. S. Phillips, V. Bourdette, and H. Teng (2010b), Uncertainty in climate change projections: The role of internal variability, *Clim. Dyn.*, *38*, 527–546, doi:10.1007/s00382-010-0977.

DiNezio, P. N., A. C. Clement, G. Vecchi, B. Soden, B. Kirtman, and S.-K. Lee (2009), Climate response of the equatorial Pacific to global warming, *J. Clim.*, *22*, 4873–4892, doi:10.1175/2009JCLI2982.1.

Dore, J. E., R. Lukas, D. W. Sadler, and D. M. Karl (2003), Climate-driven changes to the atmospheric CO_2 sink in the subtropical North Pacific Ocean, *Nature*, *424*, 754–757, doi:10.1038/nature01885.

Dore, J. E., R. Lukas, D. W. Sadler, M. J. Church, and D. M. Karl (2009), Physical and biogeochemical modulation of ocean acidification in the central North Pacific, *Proc. Natl. Acad. Sci. U. S. A.*, *106*, 12,235–12,240, doi:10.1073/pnas.0906044106.

Durack, P. J., and S. E. Wijffels (2010), Fifty-year trends in global ocean salinities and their relationship to broad-scale warming, *J. Clim.*, *23*, 4342–4362, doi:10.1175/2010JCLI3377.1.

Enfield, D. B., A. M. Mestas-Nuñez, and P. J. Trimble (2001), The Atlantic Multidecadal Oscillation and its relation to rainfall and river flows in the continental U.S., *Geophys. Res. Lett.*, *28*, 2077–2080, doi:10.1029/2000GL012745.

Gordon, C., et al. (2000), The simulation of SST, sea ice extents and ocean heat transports in a version of the Hadley Centre coupled model without flux adjustments, *Clim. Dyn.*, *16*, 147–168, doi:10.1007/s003820050010.

Gordon, H. L., et al. (2002), The CSIRO Mk3 Climate System Model, *Atmos. Res. Tech. Pap. 60*, 134 pp., Commonw. Sci. and Ind. Res. Organ., Clayton South, Victoria, Australia.

Han, W., G. A. Meehl, and A. Hu (2006), Interpretation of tropical thermocline cooling in the Indian and Pacific oceans during recent decades, *Geophys. Res. Lett.*, *33*, L23615, doi:10.1029/2006GL027982.

Held, I. M., and B. J. Soden (2006), Robust responses of the hydrological cycle to global warming, *J. Clim.*, *19*, 5686–5699, doi:10.1175/JCLI3990.1.

Hofmann, E. E. (1985), The large-scale horizontal structure of the Antarctic Circumpolar Current from FGGE drifters, *J. Geophys. Res.*, *90*, 7087–7097, doi:10.1029/JC090iC04p07087.

Holland, M. M., M. C. Serreze, and J. Stroeve (2008), The sea ice mass budget of the Arctic and its future change as simulated by coupled climate models, *Clim. Dyn.*, *34*, 185–200, doi:10.1007/s00382-008-0493-4.

Jang, C.-J., J. Park, T. Park, and S. Yoo (2011), Response of the ocean mixed layer depth to global warming and its impact on primary production: A case for the North Pacific Ocean, *ICES J. Mar. Sci.*, *68*, 996–1007, doi:10.1093/icesjms/fsr064.

Josey, S. A., E. C. Kent, and P. K. Taylor (1998), The Southampton Oceanography Center (SOC) ocean-atmosphere heat, momentum, and freshwater flux atlas, *Rep. 6*, 30 pp., Southampton Oceanogr. Cent., Southampton, U. K. [Available online at http://www.noc.soton.ac.uk/ooc/REFERENCES/PREPRINTS/SOC_flux_atlas.pdf].

Jungclaus, J. H., et al. (2006), Ocean circulation and tropical variability in the coupled model ECHAM5/MPI-OM, *J. Clim.*, *19*, 3952–3972, doi:10.1175/JCLI3827.1.

Keeling, R. F., A. Körtzinger, and N. Gruber (2010), Ocean deoxygenation in a warming world, *Annu. Rev. Mar. Sci.*, *2*, 199–229, doi:10.1146/annurev.marine.010908.163855.

Kim, S.-J., G. Flato, G. Boer, and N. McFarlane (2002), A coupled climate model simulation of the Last Glacial Maximum. Part 1: Transient multidecadal response, *Clim. Dyn.*, *19*, 515–537, doi:10.1007/s00382-002-0243-y.

Knutti, R., R. Furrer, C. Tebaldi, J. Cermak, and G. Meehl (2010), Challenges in combining projections from multiple climate models, *J. Clim.*, *23*, 2739–2758, doi:10.1175/2009JCLI3361.1.

Lin, J. (2007), The double ITCZ problem in IPCC AR4 coupled GCMs: Ocean-atmosphere feedback analysis, *J. Clim.*, *20*, 4497–4525, doi:10.1175/JCLI4272.1.

Liu, Z., S. Vavrus, F. He, N. Wen, and Y. Zhong (2005), Rethinking tropical ocean response to global warming: The enhanced equatorial warming, *J. Clim.*, *18*, 4684–4700, doi:10.1175/JCLI3579.1.

Luo, Y., and L. M. Rothstein (2009), Simulated response of North Pacific Mode Waters to global warming, *Geophys. Res. Lett.*, *36*, L23609, doi:10.1029/2009GL040906.

Mantua, N. J., S. R. Hare, Y. Zhang, J. M. Wallace, and R. Francis (1997), A Pacific interdecadal climate oscillation with impacts on salmon production, *Bull. Am. Meteorol. Soc.*, *78*, 1069–1079, doi:10.1175/1520-0477(1997)078<1069:APICOW>2.0.CO;2.

McDougall, T. J., D. A. Jackett, D. G. Wright, and R. Feistel (2003), Accurate and computationally efficient algorithm for potential temperature and density of seawater, *J. Atmos. Oceanic Technol.*, *20*, 730–741, doi:10.1175/1520-0426(2003)20<730:AACEAF>2.0.CO;2.

Meehl, G. A., C. Covey, T. Delworth, M. Latif, B. McAvaney, J. F. B. Mitchell, R. J. Stouffer, and K. E. Taylor (2007), The WCRP CMIP3 multimodel dataset: A new era in climate change research, *Bull. Am. Meteorol. Soc.*, *88*, 1383–1394, doi:10.1175/BAMS-88-9-1383.

Merryfield, W., and S. Kwon (2007), Changes in North Pacific mixed layer depth in the 20th and 21st centuries as simulated by coupled climate models, paper presented at North Pacific Marine Science Organization 16th Annual Meeting, Victoria, B. C., Canada, 26 Oct. to 6 Nov.

Nakićenović, N., et al. (2000), Summary for policymakers, in *Emissions Scenarios*, edited by N. Nakićenović and R. Swart, pp. 1–27, Cambridge Univ. Press, Cambridge, U. K.

Ono, T., T. Midorikawa, Y. W. Watanabe, K. Takodoro, and T. Saino (2001), Temporal increases of phosphate and apparent oxygen utilization in the subsurface waters of western subarctic Pacific from 1968 to 1998, *Geophys. Res. Lett.*, *28*, 3285–3288, doi:10.1029/2001GL012948.

Pierce, D. W., T. P. Barnett, B. D. Santer, and P. J. Gleckler (2009), Selecting global climate models for regional climate change studies, *Proc. Natl. Acad. Sci. U. S. A.*, *106*(21), 8441–8446, doi:10.1073/pnas.0900094106.

Polovina, J. J., E. A. Howell, and M. Abecassis (2008), Ocean's least productive waters are expanding, *Geophys. Res. Lett.*, *35*, L03618, doi:10.1029/2007GL031745.

Power, S. B., T. Casey, C. Folland, A. Colman, and V. Metha (1999), Inter-decadal modulation of the impact of ENSO on Australia, *Clim. Dyn.*, *15*, 319–324, doi:10.1007/s003820050284.

Randall, D. A., et al. (2007), Climate models and their evaluation, in *Climate Change 2007: The Physical Science Basis: Working Group I Contribution to the Fourth Assessment Report of the Intergovernmental Panel on Climate Change*, edited by S. Solomon et al., pp. 589–662, Cambridge Univ. Press, New York.

Rawlins, M. A., et al. (2010), Analysis of the Arctic System for freshwater cycle intensification: Observations and expectations, *J. Clim.*, *23*, 5715–5737, doi:10.1175/2010JCLI3421.1.

Reichler, T., and J. Kim (2008), How well do coupled models simulate today's climate?, *Bull. Am. Meteorol. Soc.*, *89*, 303–311, doi:10.1175/BAMS-89-3-303.

Richter, I., and S.-P. Xie (2010), Moisture transport from the Atlantic to the Pacific basin and its response to North Atlantic cooling and global warming, *Clim. Dyn.*, *35*, 551–566, doi:10.1007/s00382-009-0708-3.

Santer, B., et al. (2009), Incorporating model quality information in climate change detection and attribution studies, *Proc. Natl. Acad. Sci. U. S. A.*, *106*(35), 14,778–14,783, doi:10.1073/pnas.0901736106.

Sarmiento, J. L., T. M. C. Hughes, R. J. Stouffer, and S. Manabe (1998), Simulated response of the ocean carbon cycle to anthropogenic climate warming, *Nature*, *393*, 245–249, doi:10.1038/30455.

Sen Gupta, A., A. Santoso, A. S. Tashetto, C. C. Ummenhofer, M. H. England, and J. Trevena (2009), Projected changes in the Southern Hemisphere ocean and sea-ice in the IPCC-AR4 climate models, *J. Clim.*, *22*, 3047–3078, doi:10.1175/2008JCLI2827.1.

Son, S.-W., et al. (2008), The impact of stratospheric ozone recovery on the Southern Hemisphere westerly jet, *Science*, *320*, 1486–1489, doi:10.1126/science.1155939.

Steinacher, M., et al. (2010), Projected 21st century decrease in marine productivity: A multi-model analysis, *Biogeosciences*, *7*, 979–1005, doi:10.5194/bg-7-979-2010.

Stephens, G. L., and T. D. Ellis (2008), Controls of global-mean precipitation increases in global warming GCM experiments, *J. Clim.*, *21*, 6141–6155, doi:10.1175/2008JCLI2144.1.

Stramma, L., G. C. Johnson, J. Sprintall, and V. Mohrholz (2008), Expanding oxygen-minimum zones in the tropical oceans, *Science*, *320*, 655–658, doi:10.1126/science.1153847.

Tebaldi, C., and R. Knutti (2007), The use of the multi-model ensemble in probabilistic climate projections, *Philos. Trans. R. Soc. A*, *365*, 2053–2075, doi:10.1098/rsta.2007.2076.

Tebaldi, C., J. M. Arblaster, and R. Knutti (2011), Mapping model agreement in future climate projections, *Geophys. Res. Lett.*, *38*, L23701, doi:10.1029/2011GL049863.

Terray, L., L. Corre, S. Cravatte, T. Delcroix, G. Riverdin, and R. Aurelien (2012), Near-surface salinity as Nature's rain gauge to detect human influence on the tropical water cycle, *J. Clim.*, *25*, 958–977.

Valcke, S., L. Terray, and A. Piacentini (2000), The OASIS coupler user guide, version 2.4, *Tech. Rep. TR/CGMC/00-10*, 85 pp., Cent. Eur. de Rech. et de Form. Av. en Calc. Sci., Toulouse, France.

Watanabe, Y. W., M. Wakita, N. Maeda, T. Ono, and T. Gamo (2003), Synchronous bidecadal periodic changes of oxygen, phosphate and temperature between the Japan Sea deep water and the North Pacific intermediate water, *Geophys. Res. Lett.*, *30*(24), 2273, doi:10.1029/2003GL018338.

Whitney, F. A., H. J. Freeland, and M. Robert (2007), Persistently declining oxygen levels in the interior waters of the eastern subarctic Pacific, *Prog. Oceanogr.*, *75*, 179–199, doi:10.1016/j.pocean.2007.08.007.

Wilks, D. S. (1995), *Statistical Methods in the Atmospheric Sciences*, 464 pp., Academic, San Diego, Calif.

Xie, S.-P., C. Deser, G. A. Vecchi, J. Ma, H. Teng, and A. T. Wittenberg (2010), Global warming pattern formation: Sea surface temperature and rainfall, *J. Clim.*, *23*, 966–986, doi:10.1175/2009JCLI3329.1.

Yukimoto, S., et al. (2001), The new Meteorological Research Institute coupled GCM (MRICGCM 2). Model climate and variability, *Pap. Meteorol. Geophys.*, *51*, 47–88, doi:10.2467/mripapers.51.47.

M. A. Alexander, A. Capotondi, and J. D. Scott, Physical Science Division, Earth System Research Laboratories, NOAA, 325 Broadway, Boulder, CO 80305, USA. (antonietta.capotondi@noaa.gov)

N. A. Bond, Joint Institute for the Study of the Atmosphere and Ocean, University of Washington, Box 355672, Seattle, WA 98195, USA.

E. N. Curchitser, Institute of Marine and Coastal Sciences, Rutgers, State University of New Jersey, New Brunswick, NJ 08901, USA.